KTH Engineering Sciences

Mathematical Models in Cellular Biophysics

Jacob Kowalewski

Licentiate Thesis
Stockholm, Sweden 2007

TRITA-FYS 2007:33
ISSN 0280-316X
ISRN KTH/FYS/--07:33--SE
ISBN 978-91-7178-660-9

KTH AlbaNova University Center
Cell Physics
SE-106 91 Stockholm
SWEDEN

Akademisk avhandling som med tillstånd av Kungl Tekniska högskolan framlägges till offentlig granskning för avläggande av teknologie licentiatexamen i fysik tisdagen den 22 maj 2007 klockan 10.00 i FA32, AlbaNova Universitetscentrum, Roslagstullsbacken 21, Stockholm.

Tryck: Universitetsservice US AB

Abstract

Cellular biophysics deals with, among other things, transport processes within cells. This thesis presents two studies where mathematical models have been used to explain how two of these processes occur.

Cellular membranes separate cells from their exterior environment and also divide a cell into several subcellular regions. Since the 1970s lateral diffusion in these membranes has been studied, one the most important experimental techniques in these studies is *fluorescence recovery after photobleach* (FRAP). A mathematical model developed in this thesis describes how dopamine 1 receptors (D1R) diffuse in a neuronal dendritic membrane. Analytical and numerical methods have been used to solve the partial differential equations that are expressed in the model. The choice of method depends mostly on the complexity of the geometry in the model.

Calcium ions (Ca^{2+}) are known to be involved in several intracellular signaling mechanisms. One interesting concept within this field is a signaling microdomain where the inositol 1,4,5-triphosphate receptor (IP_3R) in the endoplasmic reticulum (ER) membrane physically interacts with plasma membrane proteins. This microdomain has been shown to cause the intracellular Ca^{2+} level to oscillate. The second model in this thesis describes a signaling network involving both ER membrane bound and plasma membrane Ca^{2+} channels and pumps, among them store-operated Ca^{2+} (SOC) channels. A MATLAB® toolbox was developed to implement the signaling networks and simulate its properties. This model was also implemented using *Virtual cell*.

The results show a high resemblance between the mathematical model and FRAP data in the D1R study. The model shows a distinct difference in recovery characteristics of simulated FRAP experiments on whole dendrites and dendritic spines, due to differences in geometry. The model can also explain trapping of D1R in dendritic spines.

The results of the Ca^{2+} signaling model show that stimulation of IP_3R can cause Ca^{2+} oscillations in the same frequency range as has been seen in experiments. The removing of SOC channels from the model can alter the characteristics as well as qualitative appearance of Ca^{2+} oscillations.

Sammanfattning (in Swedish)

Cellulär biofysik behandlar bland annat transportprocesser i celler. I denna avhandling presenteras två studier där matematiska modeller har använts för att förklara hur två av dess processer uppkommer.

Cellmembran separerar celler från deras yttre miljö och delar även upp en cell i flera subcellulära regioner. Sedan 1970-talet har lateral diffusion i dessa membran studerats, en av de viktigaste experimentella metoderna i dessa studier är *fluorescence recovery after photobleach* (FRAP). En matematisk modell utvecklad i denna avhandling beskriver hur dopamin 1-receptorer (D1R) diffunderar i en neural dendrits membran. Analytiska och numeriska metoder har använts för att lösa de partiella differentialekvationer som uttrycks i modellen. Valet av metod beror främst på komplexiteten hos geometrin i modellen.

Kalciumjoner (Ca^{2+}) är kända för att ingå i flera intracellulära signalmekanismer. Ett intressant koncept inom detta fält är en signalerande mikrodomän där inositol 1,4,5-trifosfatreceptorn (IP_3R) i endoplasmatiska nätverksmembranet (ER-membranet) fysiskt interagerar med proteiner i plasmamembranet. Denna mikrodomän har visats vara orsak till oscillationer i den intracellulära Ca^{2+}-nivån. Den andra modellen i denna avhandling beskriver ett signalerande nätverk där både Ca^{2+}-kanaler och pumpar bundna i ER-membranet och i plasmamembranet, däribland *store-operated* Ca^{2+}(SOC)-kanaler, ingår. Ett MATLAB®-verktyg utvecklades för att implementera signalnätverket och simulera dess egenskaper. Denna modell implementerades även i *Virtual cell*.

Resultaten visar en stark likhet mellan den matematiska modellen och FRAP-datat i D1R-studien. Modellen visar en distinkt skillnad i återhämtningsegenskaper hos simulerade FRAP-experiment på hela dendriter och dendritiska *spines*, beroende på skillnader i geometri. Modellen kan även förklara infångning av D1R i dendritiska *spines*.

Resultaten från Ca^{2+}-signaleringmodellen visar att stimulering av IP_3R kan orsaka Ca^{2+}-oscillationer inom samma frekvensområde som tidigare setts i experiment. Att ta bort SOC-kanaler från modellen kan ändra karaktär hos, såväl som den kvalitativa uppkomsten av Ca^{2+}-oscillationer.

Contents

Papers

This thesis is based on the following publications that will be referred to by their roman numerals:

I. Scott, L., Zelenin, S., Malmersjö, S., Kowalewski, J. M., Markus, E. Z., Nairn, A. C., Greengard, P., Brismar, H. & Aperia, A. *Allosteric changes of the NMDA receptor trap diffusible dopamine 1 receptors in spines*. PNAS, 2006. **103**(3): p. 762–767.

II. Kowalewski, J. M., Uhlén, P., Kitano, H. & Brismar, H. *Modeling the impact of store-operated Ca^{2+} entry on intracellular Ca^{2+} oscillations*. Mathematical Biosciences, 2006. **204**(2): p. 232–249. Reprinted with permission from Elsevier.

Contributions by the author

The candidate contributed to Paper I by creating the model together with H. Brismar. The candidate performed the calculations presented in Paper I and supplementary material. The candidate also performed part of the data analysis as described in this thesis.

Paper II describes a model which was created by the candidate together with H. Brismar and P. Uhlén. The manuscript was written by the candidate, P. Uhlén and H. Brismar. For this Paper, a MATLAB® toolbox, described in Appendix A was written by the candidate who also implemented the model and ran the computer simulations.

1 Introduction

Cellular biophysics deals with cellular transport, a process which influences the localization of molecules and ions within a cell. This can involve mobility of membrane proteins as well as the regulation of concentration gradients across cellular membranes [1].

Recently investigators in our group have proposed diffusion as a mechanism for lateral transport of dopamine 1-receptors within the membranes of neurons, and as a way for these receptors to be trapped in dendritic spines [2]. Paper I in this thesis describes experimental studies using confocal microscopy and mathematical modeling to examine and describe the mobility of these receptors. The author has developed the mathematical model in Paper I. This thesis describes how mathematical modeling is an approach to explain the process by which dopamine 1 receptors are trapped in dendritic spines. The physical concepts in this study are lateral diffusion and chemical reactions between protein molecules. Here analytical and numerical methods to solve reaction diffusion equations that describe this system are explained.

An important cellular transport process is the maintaining of ion concentration gradients across membranes. Intracellular Ca^{2+} is kept at a very low level compared to the extracellular environment, while several intracellular compartments have higher Ca^{2+} concentration than the cytoplasm. This makes Ca^{2+} an efficient messenger for intracellular signaling, the process whereby signals are transduced from an extracellular stimulus to an intracellular activity such as gene expression [3-5]. An important type of Ca^{2+} signaling is oscillations in intracellular Ca^{2+} concentration which occur due to the concerted interplay between different transport mechanisms within a cell. Paper II in this thesis examines ways to explain these mechanisms in terms of a mathematical model.

Mathematical modeling is a valuable tool, helping us to understand the mechanisms involved in biological systems. This has especially been the case within the field of Ca^{2+} dynamics. One reason for this is that modern, experimental methods in fluorescent and confocal microscopy provide accurate measures of spatiotemporal Ca^{2+} distribution in cells, making it possible to test mathematical models and biological theories. Another reason for modeling Ca^{2+} dynamics is that the dynamics in these systems are too complex to explain in simple, intuitive ways. Mathematical modeling has also been very successful in computational neuroscience and network models [1, 4, 6, 7]. The purpose of this thesis is to explore new modeling aspects of diffusion and binding of receptor proteins in neuronal membranes and intracellular Ca^{2+} dynamics in renal tubular epithelial cells.

2 Background

2.1 Cellular transport

Transport of solutes and solvents is central in biology. Such processes take place on length scales ranging from nm in subcellular compartments to tens of meters of water transport from the earth to the tops of trees.

2.1.1 Fick's laws of diffusion

The most obvious mechanism governing transport on cellular scales is diffusion, the process that transports solvents from regions of high concentration to regions of low concentration. The nature of diffusion is typically irreversible, increasing the entropy of the system. The flux of solute through a given area is given by Fick's first law of diffusion:

$$\mathbf{J} = -D\nabla c\,, \tag{2.1}$$

where ∇c is the concentration gradient. The flux vector $\mathbf{J}$ is measured in mol/(m^2·s), the SI unit of concentration is mol/m^3 or mM, and consequently the diffusion coefficient D is measured in m^2/s [1]. Combining Fick's first law with the continuity equation one obtains:

$$\nabla \cdot \mathbf{J} = -\frac{\partial c}{\partial t}\,, \tag{2.2}$$

which states that the divergence in the flux is equal to the rate of decrease in concentration. Using Gauss' theorem, this can be expressed as:

$$\iiint_V (\nabla \cdot \mathbf{J})\,dV = \oiint_S \mathbf{J} \cdot d\mathbf{S} = -\iiint_V \frac{\partial c}{\partial t}\,dV\,, \tag{2.3}$$

where $\mathbf{S}$ is the surface of the volume V. This means that the total flux through the surface of a given closed volume is equal to the rate of concentration decrease in that given volume [1]. Combining (2.1) and (2.2) gives Fick's second law, also known as the diffusion equation:

$$\frac{\partial c}{\partial t} = D\nabla^2 c\,. \tag{2.4}$$

The consequences of the equations above are illustrated in Figure 2.1.

The physical explanation of diffusion is that thermal energy induces random collisions between solute and solvent particles [8]. One can show that in the continuous limit, the location of a random walking particle, undergoing the process known as Brownian motion, will have a probability distribution equal to the concentration given by the diffusion equation [1, 9].

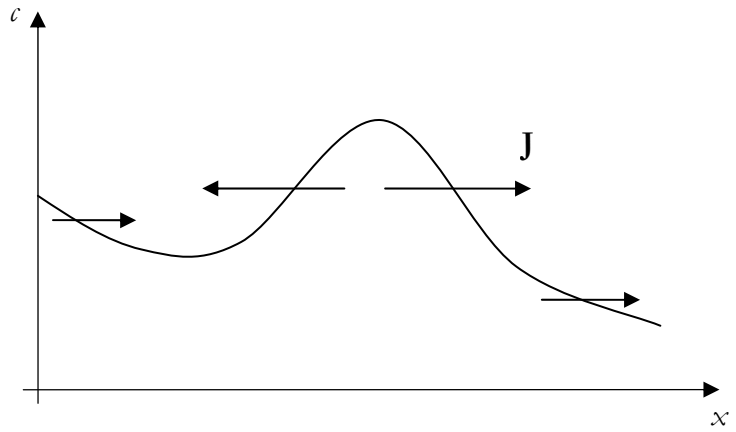

Figure 2.1 The diffusive flux **J**, indicated by the arrows, depends on the concentration c according to Equation (2.1). c is a function of the spatial coordinate x. At extreme points in concentration (maxima and minima) the flux is zero.

In real biological systems diffusion plays an important role in all kinds of passive transport, such as exchange of gases, neurotransmission and Ca^{2+} signaling. The time scale of diffusion over a certain distance is proportional to the square of that distance, making diffusion a fast process over short length scales such as synaptic clefts, but an extremely slow process over longer length scales, such as neuronal axons or the whole human body. As an example of this we can note that a synaptic cleft is approximately 10 nm in distance, this results in a 100 ns diffusion time with $D = 10^{-9}$ m^2/s [1, 10], while the same diffusion coefficient results in a 30 year diffusion time over a distance of 1 m! The concentration gradient is also an important driving force for transport across cellular membranes, and as we shall see further on in this thesis, for localization of receptor proteins in neuronal membranes.

2.1.2 Cellular membranes

The plasma membrane is the main barrier between a living cell and its exterior environment. Intracellular membranes separate organelles from the surrounding cytoplasmic environment in the cell. The concept of cellular membranes originates from the nineteenth century. Charles Ernest Overton studied cellular membranes and discovered that there is a wide variety in permeabilities across cellular membranes for different substances. Overton used this knowledge to propose that membranes are constituted of phospholipids and cholesterol. Overton's theory of a dissolve and diffuse mechanism of solutes across membranes is a simple model of membrane flux [1]. Overton also suggested that there must be an active transport mechanism to concentrate certain solutes in the intracellular environment. Overton summarized his theory in a set of rules for membrane structures [1].

Since then one has discovered that cellular membranes are composed of a phospholipid bi-layer containing large amounts of proteins which are involved in transporting ions, nutrients and other solutes. Proteins called aquaporins transport water across membranes, resulting in cell volume changes [11]. One description of the membrane structure is the fluid mosaic model which describes cellular membranes as phospholipid bi-layers containing clusters of proteins with hydrophobic interiors [12]. Other studies

have reformulated this picture into one where low mobility proteins can bind to different parts of the cytoskeleton and lipid bi-layer. This binding, known as trapping, can result from extracellular signals [13].

Lateral diffusion in membranes

One of the first studies of lateral diffusion in cellular membranes was performed by Frye and Edidin in the early 1970s [14] and was one of the main motivations of Singer and Nicolson's fluid mosaic model [12]. Frye and Edidin used immunofluorescence to study the mixture of two different proteins in cellular membranes from mouse and human cell cultures that were fused together with the Sendai virus. The two proteins were allowed to mix for 40 min and then were seen to have mixed almost completely. This mixing was proven to be decreased by lowering the temperature below 15 ºC. Also it was not affected by inhibitors of protein synthesis, of adenosine triphosphate (ATP) formation or of glutamine-dependent synthetic pathways. The diffusion coefficient was estimated to be [12]:

$$D = \frac{l^2}{2t} = 0.005\,\mu\mathrm{m}^2/\mathrm{s}\,,$$

where l = 5 μm is the distance of mixing and t = 40 min is the time that the proteins were allowed to mix.

During the mid 1970s, a new experimental method called *Fluorescence Recovery After Photobleach* (FRAP) was developed to study the mobility of membrane lipids [15]. In this method a small, fluorescent target area is bleached using strong laser light. The bleached fluorophores are thereby no longer visible, but are replaced by mobile molecules from the surrounding area in the studied object. The speed of this recovery can be used to measure the mobility of the fluorophores. Axelrod et al. [15] developed a mathematical method to fit recovery time series to a solution of an equation given by an expanded version of Fick's second law.

Axelrod et al. assume that fluorescent recovery in a region where a small subregion is bleached follows:

$$\frac{\partial c}{\partial t} = D\nabla^2 c - V_0 \frac{\partial c}{\partial x}, \tag{2.5}$$

where D is the diffusion coefficient of the fluorophore whose distribution is given by the concentration c. V_0 is the velocity of a uniform flow of fluorophores in the x-direction. Axelrod et al. provide a solution to the equation given above for a two-dimensional plane where a circular region with radius w is bleached initially. According to their solution, the mean concentration in the bleached region is given by:

$$\bar{c}(t) = C_0 \sum_{n=0}^{\infty} (-K)^n \frac{\exp\left[-\dfrac{2(t/\tau_F)^2 n}{1+n(1+2t/\tau_D)}\right]}{n!\left[1+n(1+2t/\tau_D)\right]}, \tag{2.6}$$

where K is the "amount of bleaching", given as $K \equiv \alpha T I(0)$, with α being the rate of bleaching, T the amount time during which the bleaching take place, and $I(0)$ the intensity of the bleaching radiation. τ_F and τ_D are time constants of flow and diffusion

respectively, defined as $\tau_F \equiv w / V_0$ and $\tau_D \equiv w^2 / 4D$. Axelrod et al. suggest ways to estimate the diffusion or flow rate for a circular bleaching beam by:

$$D = 0.22\frac{w^2}{\tau_{1/2}}, \quad \text{in case of diffusion,}$$

$$V_0 = 0.81\frac{w}{\tau_{1/2}}, \quad \text{in case of flow,}$$

where $\tau_{1/2}$ is the time at which the recovery has reached half of its final intensity above the initial level.

FRAP was later developed to study protein mobility in excitable membranes of neural and muscle cells, amongst others by Poo [13]. One of the main targets in the studies presented by Poo was acetylcholine (ACh) receptors. Several studies have been conducted showing that the diffusion coefficient can vary between different membrane proteins, and ranges from immobility up to around 0.5 μm^2 /s, 100 times higher than the diffusion coefficient first reported by Singer and Nicolson. The recovery of membrane protein fluorescence is often not complete which suggests that a fraction of the proteins are immobile. The mechanism behind this immobility is called trapping and can be of various origins, such as extracellular ACh receptors which are strongly concentrated close to nerve terminals in muscle membranes. The nerve terminals are thought to chemically attract the ACh receptors [13].

2.2 Intracellular signaling and calcium dynamics

All eukaryotic cells respond to signals originating from chemicals in the extracellular environment [3, 16, 17]. These chemicals can be hormones that bind to receptors in the plasma membrane. Other signaling molecules are neurotransmitters and mediators involved in local cell communication. Some signaling molecules are cell permeable and bind to intracellular receptors [18]. The process in which extracellular signals are translated into the intracellular environment is called signal transduction, which involves second messenger molecules. Common second messengers are ions such as Na^+ or Ca^{2+} [19]. Both of these ions are present in high extracellular and low intracellular concentrations [5]. In the case of Ca^{2+} the intracellular concentration is around 100 nM, while the extracellular concentration is 10,000 times higher. Ca^{2+} is also stored in intracellular organelles or compartments such as the endoplasmic reticulum (ER), which has a Ca^{2+} concentration several orders of magnitude higher than the cytosol. This organelle has a membrane which constitutes around half of the total membrane area in a eukaryotic cell [20]. Na^+ and Ca^{2+} ions access the cytosol via ion channels in a process described as passive transport. The process which transports these ions out of the cell or Ca^{2+} into the ER is called active transport.

The study of Ca^{2+} dynamics has grown tremendously as a field over the past years due to the introduction of effective dyes that make it possible to study these dynamics in real time [5]. This has also made it possible to create and test mathematical models of this phenomenon and increase our knowledge in the field [4]. The mechanisms involved in Ca^{2+} dynamics are Ca^{2+} channels in the plasma membrane and ER which can rapidly increase the cytosolic Ca^{2+} concentration and pumps in the plasma membrane and ER that decrease this concentration.

Passive transport

Since Overton's rules were formulated a large number of proteins involved in transport across cellular membrane have been discovered. Many of these transport proteins are gated or co-transporters that effectively make use of concentration gradients, ligand binding, and electrical membrane potentials to control their permeability.

The simplest possible model for transport across a cellular membrane is a description of different permeabilities for different solutes. This description is called the dissolve and diffuse-model and for a thin membrane can be summarized as:

$$J_n = P_n\left(c_n^i - c_n^o\right), \tag{2.7}$$

where J_n is the flux of a solute n through a membrane in the outward direction, c_n^i is the inside concentration of that solute, c_n^o is the outside concentration of solute n, and P_n is the permeability of that solute. The permeability is given by:

$$P_n = \frac{D_n k_n}{d}, \tag{2.8}$$

where D_n is the diffusion coefficient of solute n in the membrane, d is the thickness of the membrane, and k_n is the partition coefficient, which is the ratio between the membrane and water solubilities of solute n. Equation (2.7) is basically a special case of Fick's first law, with the membrane being in a steady state. Although the dissolve and diffuse model is a very simple description which, while not considering modern concepts of transport proteins, remains a good description of passive transport at moderate solute concentrations. However, there are many solutes that can cross the plasma membrane via pure diffusion; this includes gases such as O_2 and CO_2 as well as hydrophobic substances such as many anesthetic agents.

Passive transport gated by proteins, such as ion channels, can often be described by a modified version of (2.8), where P_n is replaced by an opening probability multiplied by the permeability of an open channel and the number of channels in the considered membrane [1, 16, 21]. Because there is a voltage across the plasma membrane, ion channel permeability will depend both on this voltage and the concentration gradient through a process called electrodiffusion. In the case of Ca^{2+} the concentration gradient is so high that it dominates over the effect of voltage [4, 21], and in this thesis the membrane voltage will not be considered as a contributing factor in Ca^{2+} dynamics.

Active transport

Some of the most energy consuming mechanisms in living cells are involved in maintaining the concentration gradients of ions across intra- and extracellular membranes. These gradients are created by transport against a concentration gradient in a process called active transport. Active transport is performed by carrier proteins that take up free energy from one reaction to lower the entropy by increasing a concentration gradient. The most common source of free energy for active transport is the dephosphorylation of adenosine-triphosphate (ATP). The membrane proteins which are involved in this transport are called pumps. Other types of active transport take up free energy from concentration gradients in processes called exchange and co-transport [16].

Many carrier proteins exploit the Na^+ gradient across the plasma membrane to actively transport other solutes uphill against their concentration gradient. Examples of this process, called secondary active transport, are the Na^+/Ca^{2+} exchanger and a Na^+-glucose cotransporter called SLGT-1 [1]. Secondary active transport does not consume ATP.

2.2.1 Calcium channels

Calcium channels are present in both the plasma membrane and intracellular membranes. They are passive transporters, often with high permeability, that are efficient because of the steep Ca^{2+} concentration gradients across these membranes. Ca^{2+} channels are opened because of a gating variable, which can be either a ligand or voltage across the membrane. An important ligand for Ca^{2+} channels in the ER membrane is inositol 1,4,5-triphosphate (IP_3), which is produced in the plasma membrane from phosphatidylinositol biphosphate (PIP_2) upon extracellular signals. IP_3 diffuses rapidly in the cytosol and binds to the IP_3 receptor (IP_3R), a ligand gated Ca^{2+} channel in the ER membrane, and thereby increases its open probability [3, 22].

In the plasma membrane, voltage operated Ca^{2+} channels (VOCs) as well as other types of Ca^{2+} channels are present. Some of these channels are gated by mechanisms that are not fully known. Polycystin-2 is a protein present in the plasma membrane which is thought to be involved in Ca^{2+} signaling caused by mechanical stimulation [23], while store operated Ca^{2+} channels (SOC) are gated by a decrease in the Ca^{2+} concentration in the ER [24].

Inositol 1,4,5-triphosphate receptor (IP_3-receptor)

IP_3R is a large protein located in the ER membrane of most eukaryotic cell types. It functions as a Ca^{2+} channel with the specific ligand IP_3. This ligand is typically produced through G protein linked receptor signaling [3, 25]. Interestingly Ca^{2+} release through IP_3R is also stimulated by Ca^{2+} itself at low concentrations. This is known as Ca^{2+} induced Ca^{2+} release (CICR), which works as a positive feedback mechanism. At higher concentrations Ca^{2+} instead works as an inhibitor for Ca^{2+} release, resulting in negative feedback. This combination of positive and negative feedback of Ca^{2+} on the IP_3R has been described as a bell shaped response curve [26].

There are three subtypes of the IP_3R, known as types 1, 2 and 3 [27]. It has been shown that these receptors show similar basic properties but have different types of regulation. IP_3R types 2 and 3 in lipid bi-layers are not inhibited by Ca^{2+} [28, 29]. However IP_3R type 3 has been shown to be so in intact cells [30]. Knockdown of specific type 1 and type 3 IP_3Rs have shown that these two receptor types play different roles in Ca^{2+} oscillations [31]. The study suggests that IP_3R type 1 maintains Ca^{2+} oscillations while IP_3R type 3 can be involved in the activation of Ca^{2+} signaling as it is not as readily inhibited as the IP_3R type 1 receptor.

Miyakawa-Naito et al. [32] have proposed a new mechanism in gating of the IP_3R. Their study showed that ouabain induced Ca^{2+} oscillations in renal proximal tubular cells are not caused by an increased level of IP_3 but by a specific physical interaction between ouabain bound Na,K-ATPase (NKA) and IP_3R. This was shown by expressing an IP_3 sponge protein, localized to the cytosol and with a high affinity for IP_3, which did not stop the Ca^{2+} oscillations. The study also showed an increased fluorescent energy transfer (FRET) between ouabain bound NKA and IP_3R. This shows that there is

approximately a 12 nm distance between the two proteins. A mutation in the NH_2-terminal of NKA abolished the Ca^{2+} oscillations, meaning that it is a probable site for the protein-protein interaction.

The complex mechanisms of the IP_3R that control the positive and negative feedback of the IP_3R is a well studied subject by both experimentalists and modelers [26, 28, 33-36]. The modeling of IP_3R was thoroughly reviewed by Sneyd and Falcke [37]. One of the first models was the De Young and Keizer model [34] which assumes that there are three independent subunits in the IP_3R. These subunits have to be in a conducting state to allow for Ca^{2+} flux. Another model is the Mak-McBride-Foskett model that is a phenomenological model in which the open probability has been fitted to measured data from IP_3R types 1 and 3 [33]. In Paper II we have compared these two models and how they are affected by store-operated Ca^{2+} channels.

Store operated calcium channels (SOC channels)

Non-excitable cells often lack voltage operated Ca^{2+} channels, but have other means to let Ca^{2+} into the cytosol. One such way, thought to be involved in Ca^{2+} oscillations, is through store-operated Ca^{2+} (SOC) channel entry. The exact mechanism involved in this kind of Ca^{2+} influx, as well as the identity of SOC channels, is not known [38]. When Ca^{2+} is released from intracellular stores it is taken up by Ca^{2+} pumps in the ER and plasma membrane of the cell. This may cause a decrease in the total amount of intracellular Ca^{2+}, which must somehow be replenished. This was modeled by Putney [39] and termed capacitative Ca^{2+} entry (CCE). At first it was thought that CCE took place through a direct link between the ER and extracellular space. It has later been shown that Ca^{2+} stores are replenished by a relatively slow increase of cytosolic Ca^{2+}, which can be pumped into the ER [38].

One important discovery was that of Ca^{2+} release activated Ca^{2+} (CRAC) current, which was shown to be highly selective for Ca^{2+} compared to some other divalent cations. This was done by whole-cell patch clamp measurements combined with ratiometric Ca^{2+} imaging that showed Ca^{2+} currents that were activated by depletion of the ER in mast cells. CRAC is today considered to be one of perhaps several SOC pathways [38, 40, 41].

It is still not known how the ER communicates Ca^{2+} depletion to the plasma membrane. At least three different qualitative explanations have been proposed [41]. One of these models describes vesicular transport, according to which SOC channels are transported in vesicles and fused into the plasma membrane. Another model suggests physical interaction between the membranes of the ER and the cell, possibly through the IP_3R. The third possible explanation was first presented by Randriamampita and Tsien [42] and includes a diffusible Ca^{2+} influx factor (CIF) that diffuses through the cytosol and activates SOC in the plasma membrane. In Paper II we have made use of the CIF explanation when modeling SOC and its impact on Ca^{2+} oscillations.

Some studies suggest that that there is a physical interaction between the IP_3R in the ER membrane and SOC channels in the plasma membrane. Mikoshiba, Gill and colleagues [43] have shown that IP_3R is required to activate SOC. These studies have suggested that transient receptor potential (TRP) channels are functionally similar to SOC channels. TRP is a large family of Ca^{2+} channels, first found in *Drosophila*, but

several members of this family have also been found in mammalian cells, amongst others, in human embryonic kidney cells [35, 43, 44].

2.2.2 Calcium pumps

The low, cytosolic Ca^{2+} concentration is maintained by active transporters, in non-excitable cells mainly by ATP consuming pumps. These pumps are found in the mitochondria, ER and plasma membranes. A well understood protein for this kind of transport is the Sarco-Endoplasmic Reticulum Ca^{2+} ATPase (SERCA). This pump consumes ATP and transports Ca^{2+} from the cytosol to the ER. A similar pump for active Ca^{2+} transport is the plasma membrane Ca^{2+} ATPase (PMCA) which pumps Ca^{2+} across the plasma membrane, out of the cell.

There are mathematical, well-established models on how the active Ca^{2+} transport works in the ER membrane, see the modeling section. These models are based on measurements of uptake of the radioactive isotope $^{45}Ca^{2+}$ into vesicles prepared from intracellular membranes. The PMCA and SERCA proteins have been crystallized and their three dimensional molecular structure is known [17, 21].

2.2.3 Calcium oscillations

A high cytosolic Ca^{2+} concentration is toxic to a cell, especially if this level is sustained for a longer period of time. As mentioned above, Ca^{2+} signaling is involved in a large number of cellular processes. Some of these processes, such as neural activity and muscle contraction are triggered by single Ca^{2+} transients, while many complex processes such as gene transcription respond to oscillating Ca^{2+} signals. Ca^{2+} oscillations can have periods ranging from seconds to days. It is believed that this diversity in frequencies, as well as amplitudes, can be an explanation of the large number of mechanisms involving Ca^{2+} signaling [5, 45-48].

The channels and pumps described above serve as ON and OFF mechanisms in Ca^{2+} signaling. One important actor in Ca^{2+} oscillations is IP_3 receptor (IP_3R), with its combination of positive and negative feedback on cytosolic Ca^{2+} levels. It is clear that Ca^{2+} oscillations are driven by a system with inertia. As we show in Paper II stimulation of the IP_3R can create a system where Ca^{2+} is released from the ER and undergoes reuptake by the SERCA pump in a periodic manner.

The most common way to activate the IP_3R is through phospholipase C via G proteins that produce IP_3 and diacylglycerol from PIP_2. IP_3 increases the open probability of the IP_3 receptor which in turn rapidly releases Ca^{2+} into the cytosol. The rate of Ca^{2+} release is at first increased through CICR, and later decreases by negative feedback. At this point the OFF processes, mainly pumps in the plasma and ER membranes begin to dominate and cause a decrease in cytosolic Ca^{2+} [49]. As mentioned above, Miyakawa-Naito et al. [32] have shown that Ca^{2+} oscillations can also be caused by a novel mechanism involving physical interaction between the Na,K-ATPase and IP_3R, without involving IP_3.

The large range of frequencies at which Ca^{2+} oscillations occur in combination with the large number of cellular processes that they are involved in make it plausible that these processes are sensitive to the frequency of Ca^{2+} oscillations. This is generally believed, but there is very little experimental evidence for this view. One important

finding in this area was made by De Koninck and Schulman [50], showing that calmodulin-dependent protein kinase II (CaM kinase II) has an activity which is highly regulated by Ca^{2+} oscillation frequency. CaM kinase II in turn affects synaptic plasticity in neurons, which is the basic principle for learning and memory, and gene transcription, the main process behind cell differentiation.

2.3 Problem statement

The aim of this thesis is to mathematically model behavior found experimentally in living cells. A necessary principle in this kind of work is to simplify the biological system in such a way that only a limited number of parameters are present. This simplification is a big part of the creation of a model, introducing a hypothesis that can be compared with experimental results. Using physical laws, a hypothesis can be formulated into a mathematical model, normally describing the studied system as differential equations. Computer simulations can numerically solve these differential equations and make it possible to compare hypothetical model results to actual experiments. Hypotheses that may seem realistic may be excluded if they make predictions that do not agree with the experimental results [21].

Paper I shows that lateral diffusion in the cell membrane is an important mechanism involved in the trapping of dopamine 1 receptors (D1R) in dendritic spines. The method used to study this movement is FRAP [13, 15], where a region of a dendrite containing a fluorescent construct called pD1R-venus is bleached by intense laser light [2]. The recovery of fluorescence is studied and can be analyzed to measure the transport properties in this system. To describe the recovery process as well as the mechanism behind the trapping of D1R in spines, a mathematical model is developed in this thesis. Analytical and numerical methods are used in this thesis to fit the experimental data of the FRAP experiments to this model.

The discovery of Ca^{2+} oscillations caused by α-haemolysin [46] and ouabain [45] have led to questions concerning the specific mechanisms involved in this type of oscillations. Experimental studies have shown that ouabain-induced oscillations are caused by a signaling microdomain with physical protein-protein interactions [32]. Paper II proposes a mathematical model with characteristics similar to these experimental results as well as a new model for store-operated Ca^{2+} entry (SOC).

3 Methods and modeling

3.1 Modeling of diffusion in cells

3.1.1 Fick's laws in *d* dimensions

In the Background of this thesis diffusion in three dimensions is described. Solving the diffusion equation in three dimensions can be a difficult problem, both analytically and numerically, because of the high number of degrees of freedom. In many biologically relevant problems the number of dimensions can be reduced to two or even one. When studying transmembrane diffusion, the concentration gradient is often one dimensional, in the direction normal to the membrane surface [1]. Lateral membrane diffusion is usually a two dimensional problem, where proteins or other substances can move in any of the dimensions parallel to the membrane surface. Let us consider a diffusion equation as given by (2.4) where a substance is free to move in a *d*-dimensional space.

To solve a partial differential equation (PDE), like the diffusion equation, two principal methods exist. When the whole space is considered Green's functions can be used. In this method the solution for a point source concentration is calculated to be:

$$c(\mathbf{r},t) = \frac{1}{(4\pi Dt)^{d/2}} e^{-r^2/4Dt}, \tag{3.1}$$

where $r = |\mathbf{r}|$ is the distance from the original point source. The concentration of a diffusing substance with an initial point source is equal to the probability distribution of a random walking particle. For an arbitrary initial concentration $c(\mathbf{r},0)$ the solution is calculated as a convolution between $c(\mathbf{r},0)$ and the Green's function given by (3.1) [9]:

$$c(\mathbf{r},t) = \int_{\mathbf{R}^d} c(\mathbf{r}',0) \frac{1}{(4\pi Dt)^{d/2}} e^{-(r-r')^2/4Dt} d^d\mathbf{r}'. \tag{3.2}$$

When a confined region of space is considered, the Green's function method is often not practical. The boundary conditions around a confined region in space make it possible to solve a PDE using the product method instead. This method reduces a PDE to a set of ordinary differential equations, which together with the boundary conditions form a set of eigenfunctions whose product can be shown to be a solution to the original PDE. The number of factors in the solution is equal to the number of degrees of freedom in the PDE. A sum of an infinite number of eigenfunctions can fulfill the initial conditions of the PDE, and thus solve the problem. This kind of method is used in Paper I to solve the FRAP problem in a dendritic spine (see below). In general the solution to the diffusion equation is given by:

$$c(\mathbf{r},t) = \sum_{n=0}^{\infty} c_n f(k_n \mathbf{r}) e^{-Dk_n^2 t}, \tag{3.3}$$

where k_n and f depend on the geometry and boundary conditions of the problem, and c_n is a series expansion of the initial concentration. For one-dimensional problems $f(k_n x)$ is a periodic function and c_n is given by the corresponding series expansion [9].

3.1.2 Solving the theoretical FRAP problem

Diffusion in dendrite

In Paper I we model the dendrite as a long cylinder. A piece of the dendrite is bleached, leading to diffusion of unbleached and bleached fluorescent molecules independently of each other. To simulate the fluorescent intensity in this system we consider the concentration of fluorescent material and assume that the fluorescent intensity is proportional to this concentration. Because the diffusion only takes place along the dimension of the symmetry axis of the cylindrical dendrite, we can view this problem as one-dimensional. If we assume that the bleached area is centered on the origin and has a length of $2l$, Fick's second law can be thus written as:

$$\frac{\partial c}{\partial t} = D\frac{\partial^2 c}{\partial x^2}, \tag{3.4}$$

with the initial condition:

$$c(x,0) = \begin{cases} C_0, & |x| \geq l \\ 0, & |x| < l \end{cases} \tag{3.5}$$

as shown in Figure 3.1a. This PDE can be solved analytically using Green's functions [1, 9] and has the solution:

$$c(x,t) = C_0\left(1 - \int_{-l}^{l} \frac{1}{\sqrt{4\pi Dt}} e^{-(x-x')^2/4Dt}\,dx'\right) = \frac{C_0}{2}\left[\operatorname{erfc}\left(\frac{x+l}{2\sqrt{Dt}}\right) + \operatorname{erfc}\left(\frac{-x+l}{2\sqrt{Dt}}\right)\right], \tag{3.6}$$

where erfc is the complementary error function defined as:

$$\operatorname{erfc}(x) = 1 - \frac{2}{\sqrt{\pi}}\int_0^x e^{-\xi^2}\,d\xi .$$

The solution is shown in Figure 3.1b.

When doing FRAP studies the mean fluorescence intensity in the bleached area as a function of time is measured. Under the assumption that fluorescence intensity is proportional to concentration, using the substitution $a = D/l^2$, this quantity can be calculated as:

$$\bar{c}(t) = \frac{1}{2l}\int_{-l}^{l} c(x,t)dx = C_0\left(\sqrt{\frac{at}{\pi}}\left(1 - e^{-1/at}\right) + erfc\left(1/\sqrt{at}\right)\right). \tag{3.7}$$

This expression could be fitted to a measured recovery curve using nonlinear least-square optimization. However, the measured recovery curve is influenced by focus drift caused by small movements of the dendrite. Because the study is done in a confocal microscope, focus drift has a large impact on the recovery curve. It is often not possible to fit the data well to the expression given by Equation (3.7). A quantity which is less influenced by focus drift is the half time of the recovery, $t_{1/2}$. This is the time from the

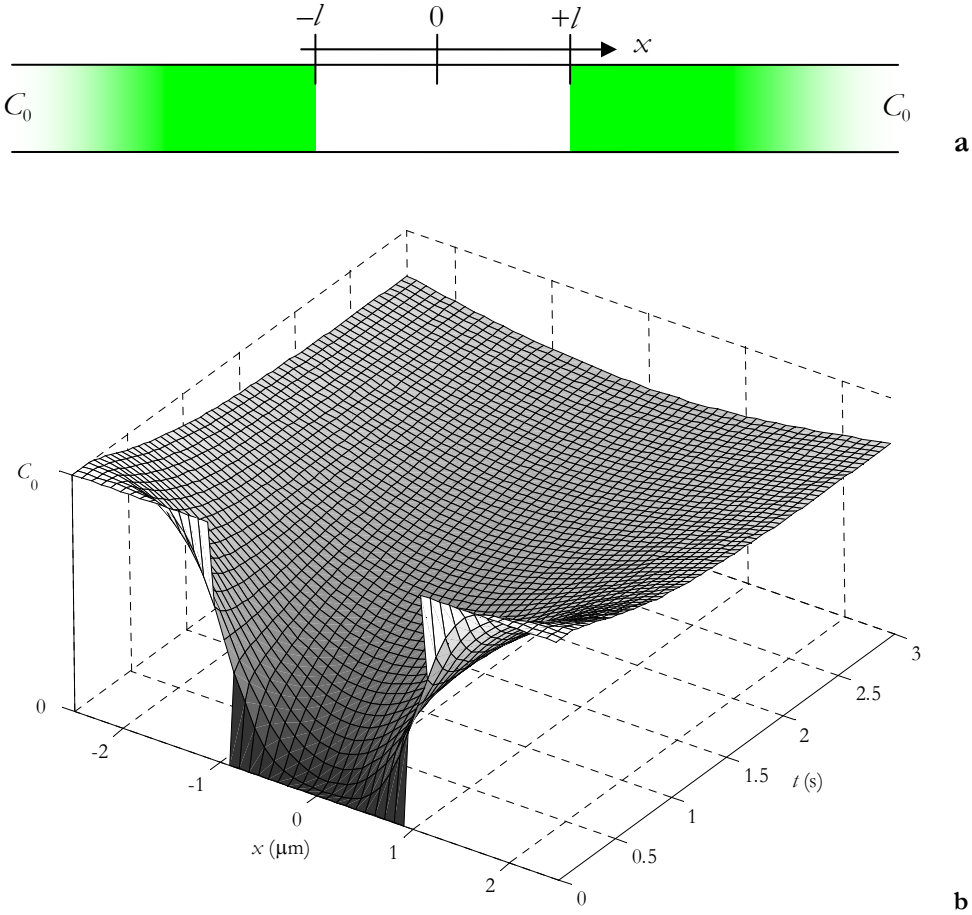

Figure 3.1 (a)The initial condition and (b) analytical solution for the FRAP problem of a dendrite as given by Equation (3.6). The parameters in the solution are D = 1 μm²/s and l = 1

beginning of the recovery until the intensity has reached half of its final recovery value. This intensity is given by $I_{1/2} = I_i + (I_e - I_i)/2$, where I_i is the intensity after photobleach and I_e is the intensity at the end of the recovery as shown in Supporting Figure 9 in Paper I. To calculate $t_{1/2}$ we identify $\bar{c}(t)$ given by (3.7) as a function of at and numerically solve the equation:

$$\frac{1}{2} = \sqrt{\frac{at_{1/2}}{\pi}}\left(1 - e^{-1/at_{1/2}}\right) + erfc\left(1/\sqrt{at}_{1/2}\right),$$

which gives the result: $at_{1/2} \approx 0.925$. Thereby the diffusion coefficient can be calculated as:

$$D = 0.925\frac{l^2}{t_{1/2}}. \tag{3.8}$$

Diffusion in spines

A FRAP experiment in a dendritic spine can be described as diffusion in a small tube with a closed end, through which the flux of fluorophores is zero. In the other end of the tube is the dendrite, which is much larger than the spine, see Figure 3.2a. The dendrite can thus be viewed as a non-emptying pool. At the connection between the dendrite and the spine the fluorophore concentration is considered to be constantly equal

to C_0. These two boundary conditions combined with Fick's second law leads to a one-dimensional diffusion problem in a confined region. Using a series expansion that fulfills the boundary conditions and Equation (3.3), the solution to this problem can be written as:

$$c(x,t) = C_0 - \frac{4C_0}{\pi}\sum_{n=0}^{\infty}\sin\left(\frac{(1+2n)}{4l}\pi x\right)\frac{e^{-D(1+2n)^2\pi^2 t/(16l^2)}}{(1+2n)}, \tag{3.9}$$

where x is the coordinate along the axis of the spine. The length of the spine, and thereby also the bleached region, is $2l$. The solution is shown in Figure 3.2b. When taking the mean concentration over the bleached area in the same way as was done above for the dendrite, the solution becomes:

$$\frac{1}{2l}\int_0^{2l} c(x,t)dx = C_0 - \frac{8C_0}{\pi^2}\sum_{n=0}^{\infty}\left[\frac{1}{(1+2n)^2}e^{-D(1+2n)^2\pi^2 t/(16l^2)}\right]. \tag{3.10}$$

Supporting Figure 8 in Paper I compares the results of Equations (3.7) and (3.10), showing that the recovery in a spine is faster than in a dendrite.

The time $t_{1/2}$ can be calculated as above by numerically solving the equation:

$$\frac{1}{2} = 1 - \frac{8}{\pi^2}\sum_{n=0}^{10}\left[\frac{1}{(1+2n)^2}e^{-D(1+2n)^2\pi^2 t/(16l^2)}\right]. \tag{3.11}$$

The right hand side of this equation is the first 11 terms of the expression for the mean concentration divided by C_0.
This gives the result:

$$D = 0.788\frac{l^2}{t_{1/2}}. \tag{3.12}$$

A more accurate model can be made when assuming that diffusion of the fluorophore into the spine depletes the concentration of fluorophore in the dendrite. This makes the problem two-dimensional and it cannot easily be solved analytically. Therefore COMSOL Multiphysics™ (Comsol AB, Stockholm, Sweden) has been used to numerically simulate this problem using a finite element method (FEM). There is no exact, simple relationship between the half time of recovery and the diffusion coefficient in this model, but a first order approximation when l is near 375 nm and $t_{1/2}$ is near 1 s is found to be:

$$D = 1.296\frac{l^2}{t_{1/2}}, \tag{3.13}$$

where l is half the length of the spine.

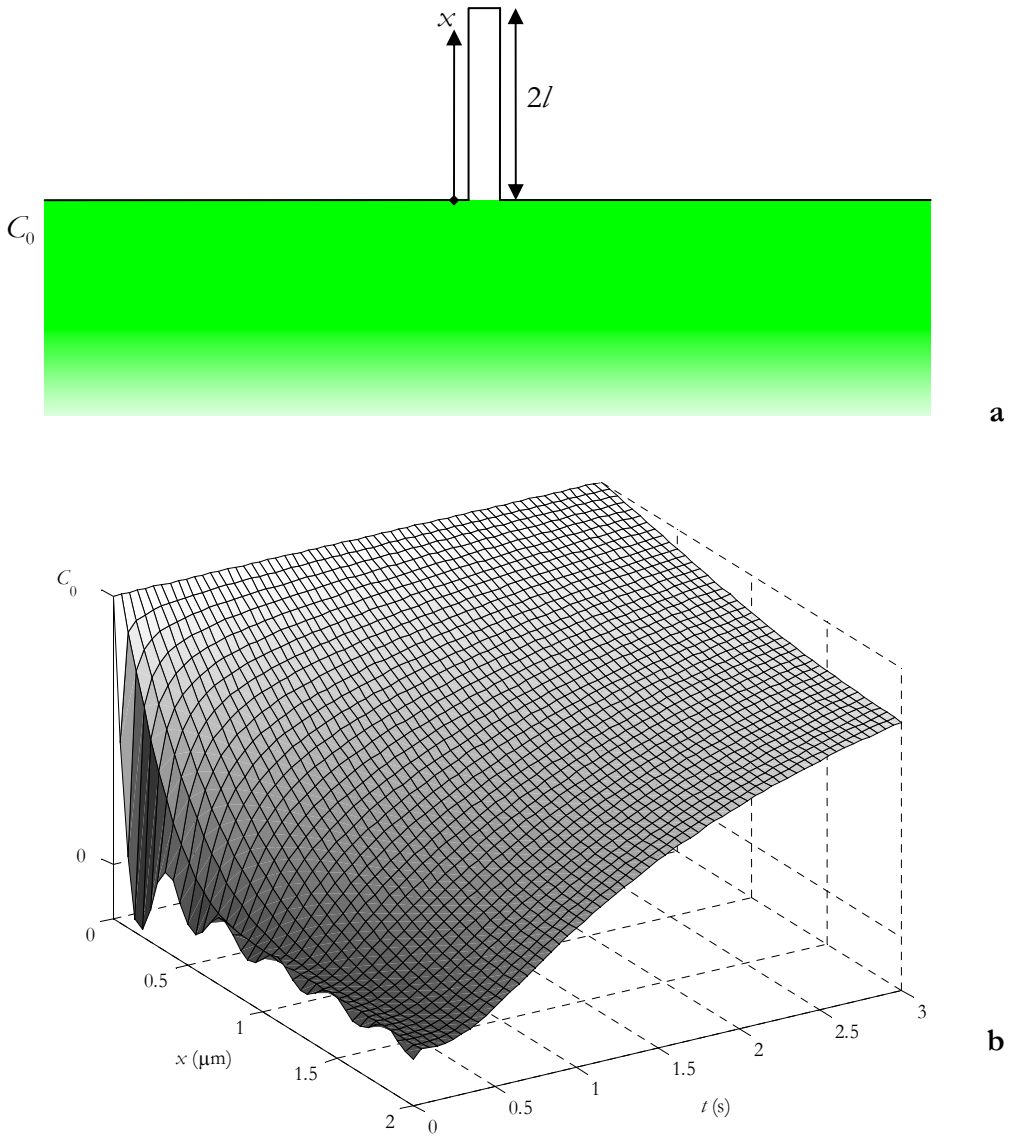

Figure 3.2 The initial condition (a) and analytical solution (b) of the FRAP problem for a spine given by the first 11 terms in Equation (3.9). The limited number of terms gives rise to the oscillatory behavior known as Gibbs phenomenon seen to the left in the picture [9]. The parameters are the same as in Figure 3.1.

3.2 Trapping of dopamine 1 receptors in spines

The trapping of diffusing dopamine 1 receptors (D1R) by N-methyl-D-aspartate (NMDA) receptors can be described by a diffusion reaction equation given by Fick's second law and an additional reaction term, R. In two dimensions this reaction diffusion equation is given by:

$$\frac{\partial c}{\partial t} = D\left(\frac{\partial^2 c}{\partial x^2} + \frac{\partial^2 c}{\partial y^2}\right) + R\,, \tag{3.14}$$

where R is the reaction rate for a species with concentration c. In the current model it has been assumed that there are two diffusing species present. One is the D1R, having a

concentration c_1, and the other species, with concentration c_2, is D1R bound to the NMDA receptor. This leads to a system of differential equations:

$$\begin{aligned}\frac{\partial c_1}{\partial t} &= D_1\left(\frac{\partial^2 c_1}{\partial x^2}+\frac{\partial^2 c_1}{\partial y^2}\right)+R_1,\\ \frac{\partial c_2}{\partial t} &= D_2\left(\frac{\partial^2 c_2}{\partial x^2}+\frac{\partial^2 c_2}{\partial y^2}\right)+R_2,\end{aligned} \tag{3.15}$$

where $R_1 = -R_2$. This means that the reactions taking place are binding and dissociation between the bound and unbound states. The model of the reactions can be described as:

$$R_2 = -R_1 = \begin{cases} k_a(c_{\max}-c_2)c_1 - k_d c_2, & \text{in the spine head } (y > 0.75\,\mu\text{m}),\\ -k_d c_2, & \text{elsewhere,}\end{cases} \tag{3.16}$$

where k_a is the binding rate and k_d is the dissociation rate in the reactions. The binding only takes place in the head of the spine while the dissociation can occur everywhere in the cell. $c_{\max}$ is the binding site concentration in the spine head. The model has been simulated using a Finite Element method (FEM) in COMSOL Multiphysics where it has been mapped onto an analytical geometry, see Figure 3.3.

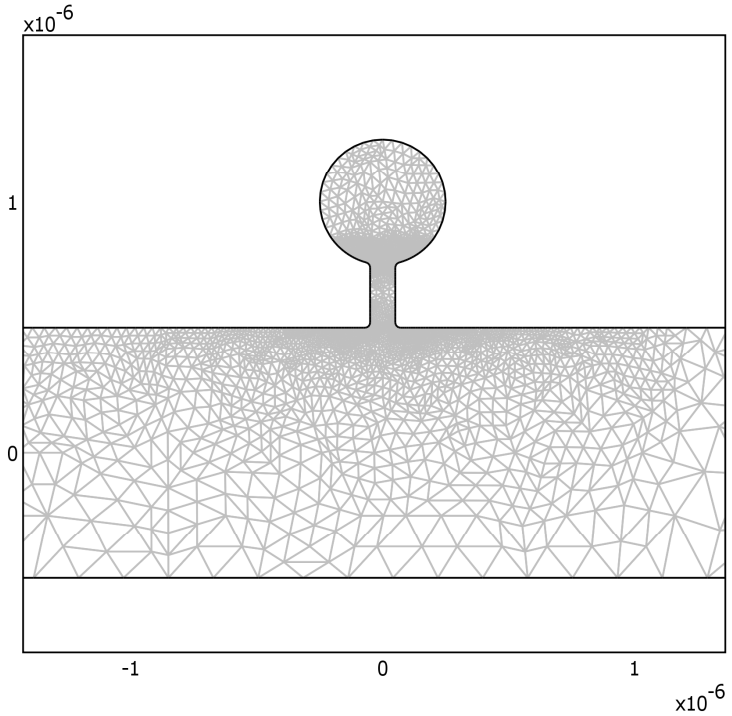

Figure 3.3 The geometry of the FEM model of the spine and the dendrite. The grey mesh shows the discretization used by the FEM solver. The geometry is described by a 1 μm wide, long dendrite with a spine that consists of a 0.10 μm wide and 0.25 μm long tube connected to a circle with a radius of 0.25 μm (the spine head). The spine head is centered at the coordinates (0,1 μm). The scales on the axes are in meters.

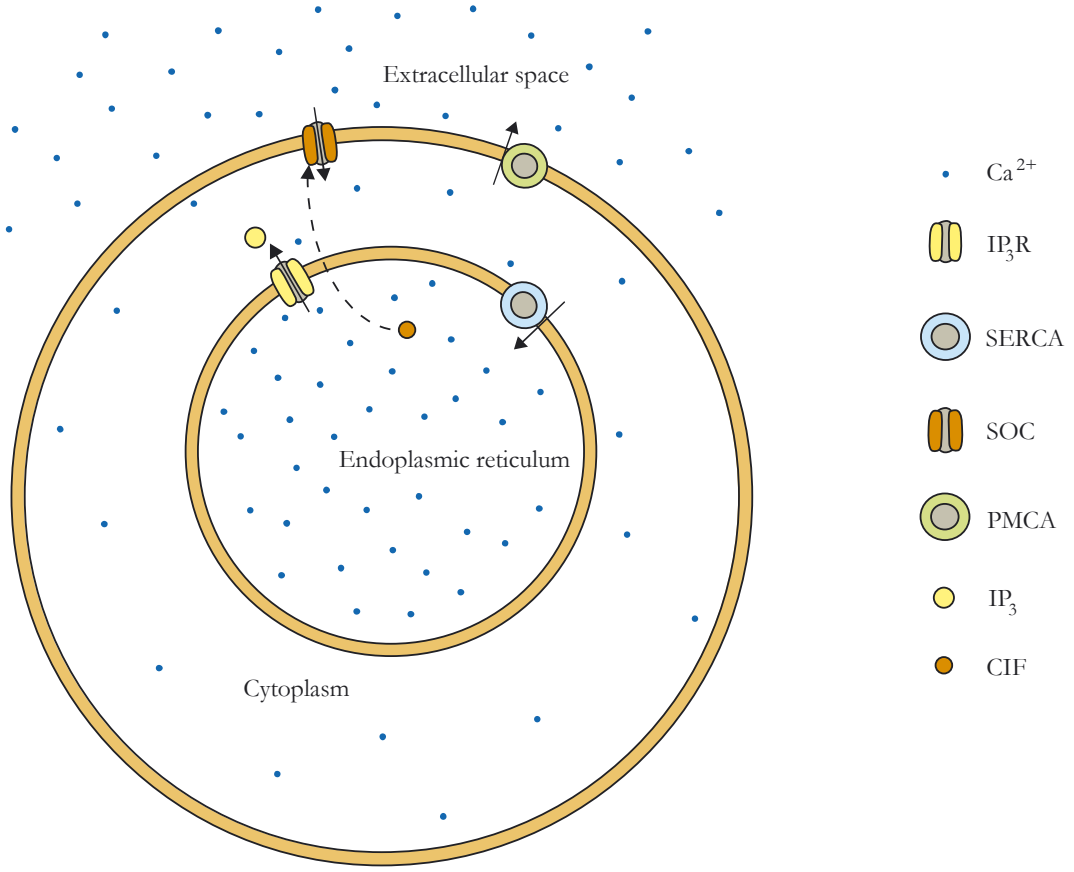

Figure 3.4 A Summary of the Ca^{2+} signaling model shows three compartments that are present in the model. The density of Ca^{2+} ions represents relative differences in Ca^{2+} concentration. Graphics by Linda Westin.

3.3 Modeling of calcium signaling

In Paper II we have created a compartmental mathematical model of a cell. The model contains a cytosolic compartment, an endoplasmic reticulum (ER) and an extracellular environment. As the extracellular environment is large and has a very high Ca^{2+} concentration it can be viewed as a non-emptying source of Ca^{2+}. In the model presented in Paper II the compartments are assumed to be well-stirred with uniform concentrations that are only dependent on time [1, 4, 51, 52]. The model is summarized in Figure 3.4.

A more detailed way to model cellular dynamics is to construct a spatial model where the mixing time is limited by diffusion [53]. In this kind of model, the concentration of a substance n with concentration c_n is described by a modified version of the diffusion equation known as the reaction diffusion equation [54].

$$\frac{\partial c_n}{\partial t} = D\frac{\partial^2 c_n}{\partial x^2} + j(x, y, z, c_n, c_m, \ldots), \tag{3.17}$$

where j is the rate of reactions that consume or produce the substance n. j can depend on a number of different quantities such as c_n, spatial coordinates or the concentration of other substances, for example c_m. A flux, through a membrane, between two different

compartments is given as a Neumann boundary condition at the location of that membrane [55]:

$$\hat{\mathbf{n}}_{\text{membrane}} \cdot D_n \nabla c_n = \alpha_{\text{transporter}}(x, y, z) J_n, \tag{3.18}$$

where $\hat{\mathbf{n}}_{\text{membrane}}$ is the unit vector normal to the membrane, $\alpha_{\text{transporter}}$ is the distribution of transporters of substance n and J_n is the flux of that substance n through these transporters. This boundary condition is a special case of Fick's first law given by equation (2.1). A well-stirred or compartmental model can be viewed as a spatial model in the limit where the diffusion coefficients are considered large enough to assume that the time scale of diffusion is much shorter than the time scale of change in concentration by flux of reactions. In a well-stirred compartmental model the equations (3.17) and (3.18) can be summed into [1]:

$$\frac{dc_n}{dt} = j(c_n, c_m, \ldots) + \frac{A_{\text{membrane}}}{V_{\text{compartment}}} J_n, \tag{3.19}$$

where $A_{\text{membrane}}/V_{\text{compartment}}$ is the surface to volume ratio of the compartment where c_n is measured. This description significantly reduces the complexity of the problem.

Ca^{2+} signaling is modeled as a combination of ON and OFF mechanisms working together to create a signal. This signal may be either a steady increase in cytosolic Ca^{2+} concentration, a transient increase, where the cytosolic Ca^{2+} returns to base level after some time or an oscillating signal [5, 47]. In a mathematical model the ON and OFF mechanism are described as terms contributing to the total flux of Ca^{2+}, $J_{Ca^{2+}}$. The three compartments that have been considered in our model are the cytosol, the endoplasmic reticulum (ER) and the extracellular (EC) environment, each one having a certain Ca^{2+} concentration. A compartmental model of this system can be written as a system of ordinary differential equations (ODEs). The model which is described in detail in Appendix A contains eight different concentrations, and ten reactions or fluxes, which can be summed into a system of ODEs using a generalized form of equation (3.19) [56]:

$$\frac{d\mathbf{S}}{dt} = \mathbf{N}\mathbf{j}, \tag{3.20}$$

where **S** is a column vector of all the species in the model, **N** is the 8×10 stoichiometry matrix and **j** is a column vector of all reactions of fluxes in the model. The rows in **j** that contain fluxes have to be multiplied by the surface to volume ratio as described by equation (3.19). This has been done using the *OOR toolbox*, which automatically can calculate the matrix **N**, by specifying the species and reactions between them, as well as the volume of each compartment present in the model. The toolbox was made using MATLAB®, see Appendix A.

To summarize the compartmental model in Paper II: it consists of a species vector:

$$\mathbf{s} = \begin{pmatrix} [\mathrm{Ca}^{2+}]_{\mathrm{cyt}} \\ [\mathrm{Ca}^{2+}]_{\mathrm{ER}} \\ [\mathrm{Ca}^{2+}]_{\mathrm{EC}} \\ [\mathrm{IP}_3]_{\mathrm{cyt}} \\ [\mathrm{G}]_{\mathrm{cyt}} \\ [\mathrm{CIF}]_{\mathrm{cyt}} \\ [\mathrm{CIF}]_{\mathrm{ER}} \\ [\mathrm{SOC}]_{\mathrm{PM}} \end{pmatrix}, \tag{3.21}$$

where the first four elements are the concentrations of Ca^{2+} and IP_3 present in the three compartments of the model. The other four species are described below as they take part in the dynamics of IP_3 and the SOC channels. The reaction vector:

$$\mathbf{j} = \left(J_{\mathrm{PMCA}}, J_{\mathrm{SERCA}}, J_{\mathrm{IP_3R}}, J_{\mathrm{SOC}}, j_G, j_{\mathrm{IP_3}}, j_{\mathrm{CIF\,prod}}, j_{\mathrm{SOC\,bindning}}, j_{\mathrm{SOC\,deg}}, J_{\mathrm{CIF}}\right)^T \tag{3.22}$$

contains the ten fluxes and reaction rates that are described below. Figure 3.4 shows a representation of the species and transporters present in the model.

In Equation (3.22) j_G and $j_{\mathrm{IP_3}}$ are reaction rates involved in the negative feedback mechanism of Ca^{2+} on the level of IP_3. This mechanism has previously been reported [52, 57, 58]. In our model it has been implemented as a reaction starting at time t_0 which produces IP_3 at a rate:

$$j_{\mathrm{IP_3}} = G_{\mathrm{signal}} I_{\mathrm{deg}} [\mathrm{IP_3}]_{\mathrm{max}} - I_{\mathrm{deg}} [\mathrm{IP_3}]_{\mathrm{cyt}} . \tag{3.23}$$

G_{signal} depends on a hypothetical substance G which is produced and degraded at a rate:

$$j_G = k_G [\mathrm{Ca}^{2+}]_{\mathrm{cyt}} - I_G [\mathrm{G}]_{\mathrm{cyt}} , \tag{3.24}$$

$$G_{\mathrm{signal}} = 1 - \frac{[\mathrm{G}]_{\mathrm{cyt}}{}^{n}}{[\mathrm{G}]_{\mathrm{cyt}}{}^{n} + K_{1/2}{}^{n}} . \tag{3.25}$$

The parameters in the equations above are defined in Paper II, Table 1.

3.3.1 Calcium channels

Ca^{2+} channels are passive transporters of Ca^{2+} that open and close with certain probabilities. The general form of flux through a Ca^{2+} channel is, as given by (2.7):

$$J_{\mathrm{Ca}^{2+}} = P_{Ca^{2+}} \left([\mathrm{Ca}^{2+}]_i - [\mathrm{Ca}^{2+}]_o \right). \tag{3.26}$$

The permeability of the channels, $P_{Ca^{2+}}$, is given as a product of the permeability of a single open channel, the number of channels in the membrane and the open probability of a single channel.

IP_3-receptors

As described in the background of this thesis there are several models of IP_3R. In our study we have compared two different models. Both of these models follow the general expression:

$$J_{IP_3R} = \left(V_{IP_3R} + V_{leak\ ER}\right)\left([Ca^{2+}]_{ER} - [Ca^{2+}]_{cyt}\right), \tag{3.27}$$

where V_{IP_3R} and $V_{leak\ ER}$ are the permeabilities of the IP_3R by regulated flux and leak respectively. The De Young and Keizer [34] model is not specific to any subtype of IP_3R and according to this model:

$$V_{IP_3R} = v_1\left[\frac{\left[Ca^{2+}\right]_{cyt}\left[IP_3\right]_{cyt} d_2}{\left(\left[Ca^{2+}\right]_{cyt}\left[IP_3\right]_{cyt} + \left[IP_3\right]_{cyt} d_2 + d_1 d_2 + \left[Ca^{2+}\right]_{cyt} d_3\right)\left(\left[Ca^{2+}\right]_{cyt} + d_5\right)}\right]^3. \tag{3.28}$$

The parameters in this model are explained in Paper II, Table 3.

The second IP_3R model was proposed by Mak et al. [33] and is described by the equations:

$$V_{IP_3R} = v_{IP_3R}\left[1 + \left(\frac{K_{act}}{\left[Ca^{2+}\right]_{cyt}}\right)\right]^{-1}\left[1 + \left(\frac{\left[Ca^{2+}\right]_{cyt}}{K_{inh}}\right)\right]^{-1}, \tag{3.29}$$

where

$$K_{inh} = \left[1 + \left(\frac{K_{IP_3}}{[IP_3]_{cyt}}\right)^{H_{IP_3}}\right]^{-1}. \tag{3.30}$$

Again, the parameters are described in Paper II, Table 3.

SOC channels

In Paper II we propose a phenomenological model of SOC channel activation. This model involves a diffusible Ca^{2+} influx factor (CIF) which is released from the ER and binds to a channel in the plasma membrane. The model suggests that CIF slowly binds to and opens SOC channels; these channels are in turn deactivated after some time given by the coefficient I_{SOC}. The flux of CIF across the ER membrane is controlled by the Ca^{2+} concentration in the ER lumen. When this concentration falls below a certain value, CIF is released into the cytosol. CIF is regenerated in the ER up to the level $[CIF]_{max}$. In Equation (3.22) J_{SOC} is the Ca^{2+} flux through the SOC channels, J_{CIF} is the flux of CIF across the ER membrane, $j_{CIF\ prod}$ is the production rate of CIF through the regeneration process, $j_{SOC\ binding}$ is the binding rate of CIF to the SOC channels and $j_{SOC\ deg}$ the deactivation rate of SOC channels in the plasma membrane. These quantities are coupled through Equation (3.20) as described in detail in Appendix A. The mathematical definition of the Ca^{2+} flux through SOC is given by:

$$J_{SOC} = (V_{SOC} + V_{leak\ PM})\left([Ca^{2+}]_{EC} - [Ca^{2+}]_{cyt}\right), \quad V_{SOC} = v_{SOC}[SOC]_{PM}, \tag{3.31}$$

where V_{SOC} is the SOC channels permeability. The flux of CIF across the ER membrane is given by:

$$J_{\mathrm{CIF}} = \begin{cases} v_{\mathrm{CIF}}\left([\mathrm{CIF}]_{\mathrm{ER}} - [\mathrm{CIF}]_{\mathrm{cyt}}\right), & \text{if } [\mathrm{Ca}^{2+}]_{\mathrm{ER}} < [\mathrm{Ca}^{2+}]_{\mathrm{ER,min}}, \\ 0 & \text{otherwise.} \end{cases} \tag{3.32}$$

The reaction rates involved in the regulations of CIF and SOC channels are given by:

$$j_{\mathrm{CIF\,prod}} = k_{\mathrm{CIF}}\left([\mathrm{CIF}]_{\mathrm{max}} - [\mathrm{CIF}]_{\mathrm{ER}}\right), \tag{3.33}$$

$$j_{\mathrm{SOC\,binding}} = k_{\mathrm{SOC}}[\mathrm{CIF}]_{\mathrm{cyt}}, \quad j_{\mathrm{SOC\,deg}} = -I_{\mathrm{SOC}}[\mathrm{SOC}]_{\mathrm{PM}}. \tag{3.34}$$

See Paper II, Table 3 for definitions of the parameters.

3.3.2 Calcium pumps

The activities of the Ca^{2+} pumps were implemented as in Baker et al. [51]. The SERCA and PMCA activities are thus:

$$J_{\mathrm{SERCA}} = \frac{V_{\mathrm{max,SERCA}}[\mathrm{Ca}^{2+}]_{\mathrm{cyt}}{}^{n_{\mathrm{SERCA}}}}{[\mathrm{Ca}^{2+}]_{\mathrm{cyt}}{}^{n_{\mathrm{SERCA}}} + K_{1/2,\mathrm{SERCA}}{}^{n_{\mathrm{SERCA}}}}, \tag{3.35}$$

$$J_{\mathrm{PMCA}} = \frac{V_{\mathrm{max,PMCA}}[\mathrm{Ca}^{2+}]_{\mathrm{cyt}}{}^{n_{\mathrm{PMCA}}}}{[\mathrm{Ca}^{2+}]_{\mathrm{cyt}}{}^{n_{\mathrm{PMCA}}} + K_{1/2,\mathrm{PMCA}}{}^{n_{\mathrm{PMCA}}}}. \tag{3.36}$$

The parameters in these expressions are found in Paper II, Table 4.

3.3.3 Calcium oscillation models

To model Ca^{2+} oscillations the parameter $[IP_3]_{max}$ was varied. This corresponds to a varied degree of stimulation of the IP_3R that has been shown in experimental studies in both experimental and modeling studies to result in Ca^{2+} oscillations [7, 32, 52]. In the present model Ca^{2+} oscillations were induced by increasing the $[IP_3]_{max}$ after the resting time t_0 which was set to 500 s. The maximum IP_3 concentration was varied in a range between 1 and 80 nM. In the model, other variations that have been implemented were to inhibit SERCA and to remove SOC channels from the model.

3.4 Numerical computation

A system of differential equations can be solved using numerical methods where the problem is discretized in a way where the solution can be described by a limited number of values at different points in space and time [54].

3.4.1 Compartmental models

A compartmental model describes a cell as a system of compartments where the concentration in each compartment is homogeneous at all times. As the concentration of species in the compartments varies in time, but is independent of space, this system can be modeled using ordinary differential equations (ODEs) [54].

As described in Appendix A, the system of ODEs was coupled and solved using the Matlab® **`ode15s`** function [59, 60]. This is a variable order, multistep solver that uses numerical differentiation formulas. It can handle stiff problems where the problem contains several different time scales [61]. Physically, the short time scale corresponds to

sudden opening of Ca^{2+} channels and the long time scale to the time at which the cell is in nearly steady state.

3.4.2 Spatial models

A computational tool that is specialized in solving a system of reaction diffusion equations is *Virtual Cell* [54, 62]. By using this program, the Ca^{2+} signaling model described by Equations (3.23)–(3.36) was entered and coupled according to Equations (3.17)–(3.18). A geometry based on data from an image of a COS-7 cell taken by a confocal microscope was added to the model, see Section 4.2.2. This resulted in a system of PDEs which was solved using simulations based on the finite volume method. Using this method, the geometry is discretized into two or three dimensional rectangular spaces, or volume elements. Within each element, the change of concentration of a species is the sum of flux and production through reactions in this element. *Virtual Cell* uses a constant time step to numerically integrate the resulting equations [54, 55].

3.5 Experimental verification by fluorescence microscopy

Fluorescent microscopy is a powerful and sensitive technique for real time live cell measurements. Using this method images of cells are recorded by using short wavelength excitation light and detecting longer wavelength emission light with a camera or photomultiplier tube (PMT).

A special type of fluorescent microscopes is the laser scanning confocal microscope in which focused laser light is used for excitation; emitted light passes a pinhole and is detected by a PMT. This makes it possible to resolve images in three dimensions. The spatial resolution of a fluorescent microscope is ideally given by the diffraction limit and is approximately equal to half the wavelength of the emission light.

3.5.1 Fluorescence recovery after photobleach

Fluorescence recovery after photobleach (FRAP) is a method using confocal microscopy to bleach a limited area in the sample. Using this method, the influx of unbleached fluorescent material, known as fluorescence recovery, is studied. In Paper I FRAP has been used to study the movement of dopamine 1 receptors (D1R) in dendrites. Neurons in organotypic striatal cultures were transfected with the fluorescent protein Venus tagged to D1R. An approximately 10 μm long region of the dendrite in a transfected neuron was bleached and the images of the recovery were collected for 5 min by recording a frame every 5 s [2, 63, 64]. Figure 3.5 shows the principle of a confocal microscope.

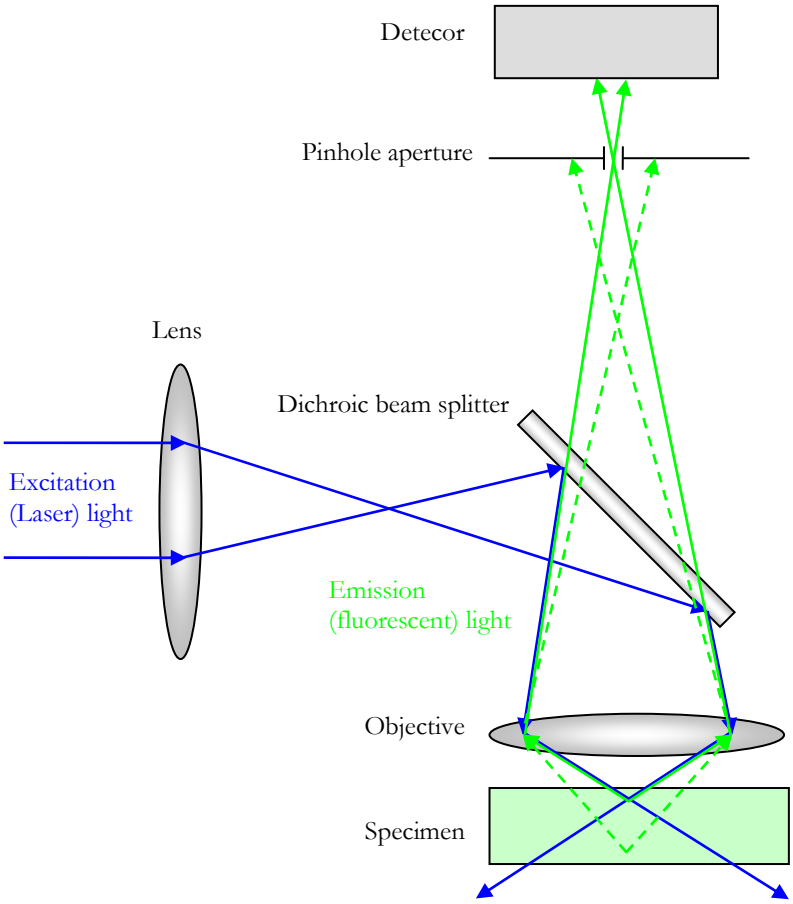

Figure 3.5 This principal drawing of a confocal microscope shows how a laser is focused onto the fluorescent specimen. The short wavelength excitation light is reflected by the beam splitter and focused onto the specimen. In focus emission light (solid line) follows the same path through the objective but passes the beam splitter and is focused onto the pinhole aperture. Out of focus emission light (dashed line) will not pass the pinhole aperture and will therefore not be detected.

The fluorescent signal from the area that had previously been bleached was averaged in each frame and plotted as a function of time. The resulting data is known as the recovery curve and was compared to the theoretical values given by Equation (3.7) as described in Section 3.1.2. From recovery curves resembling the theoretical model the diffusion coefficient was calculated using Equation (3.8).

3.5.2 Ratiometric measurements of intracellular calcium

Using fluorescent dyes such as Fura-2, intracellular Ca^{2+} concentrations can be measured. This is done by measuring the ratio of fluorescent intensity at two different excitation wavelengths. In Paper II cells were incubated with Fura-2. During measurements, each image was recorded by exciting in turn using 340 and 380 nm UV light. The images were detected by a Charge Coupled Device (CCD) camera at 510 nm. The absolute intracellular, time dependent Ca^{2+} concentration in such a recording can be calculated by:

$$\left[Ca^{2+}\right] = K_D \frac{R(t) - R_{\min}}{R_{\max} - R(t)} \cdot \frac{F_0}{F_s}, \qquad (3.37)$$

where $R(t)$ is the intensity of an image excited by 340 nm at time t pixelwise divided by the image excited by 380 nm at approximately the same time; R_{min} and R_{max} are the same ratios calculated at minimum and saturated intracellular Ca^{2+} concentrations. F_0 and F_s are the intensities of images excited by 380 nm at minimum and saturated Ca^{2+} concentrations; K_D is the dissociation constant of Ca^{2+} and Fura-2, approximately equal to 225 nM [5, 46, 65].

4 Results

4.1 Trapping of dopamine 1 receptors in neuronal spines

4.1.1 The effective diffusion coefficient of D1R in dendrites

Comparing the analytical solution of the diffusion equation for a dendritic spine with the bleached region given by $2l$ in Equation (3.7) to experimental data shows a strong similarity. Recovery curves from a number of experiments were fitted to the equation using a non-linear least-square regression method by applying the MATLAB® optimization toolbox function **`lsqcurvefit`**, which uses the Levenberg-Marquardt algorithm to fit a curve to the recovery data. The parameters that are calculated by the curve fitting are the diffusion coefficient, the mobile fraction of diffusing receptors and the intensity directly after photobleach. Because a large fraction of the recovery data curves contained focus drift, which influences the fluorescent intensity in a way completely independent of the diffusion properties of the sample, another method based on the half time of recovery and Equation (3.8) was selected instead. The diffusion coefficient calculated in this way from a large set of recovery data was shown to be 0.80 ± 0.13 $\mu m^2/s$ [2]. Figure 4.1 shows a typical FRAP experiment on a dendrite, with a theoretical recovery curve fitted to the data.

In Paper I the fluorescent recovery in a dendrite is compared to that of a spine according to the model presented in Section 3.1.2. The recovery of fluorescence in a spine is more rapid than in a dendrite, especially by the end of the recovery curve. Figure 4.2 shows a similar comparison, and also includes the simulated recovery from COMSOL Multiphysics. As can be seen when comparing Equations (3.8), (3.12) and (3.13) the half time of recovery is shortest for the analytical model of the spine, longer for the dendrite, and longest in case of the numerically simulated 2D model of the spine. By the end of the recovery, the 2D model of the spine gains speed compared to the dendrite. This can be understood in terms of fluorescent material being recruited from both directions into the bleached region. In the spine, fluorescent material only enters the region from one direction, but it is not depleted outside of the bleached region to the same extent as in the case of the dendrite. The reason for this is the difference in size between the comparatively large dendrite and the small spine.

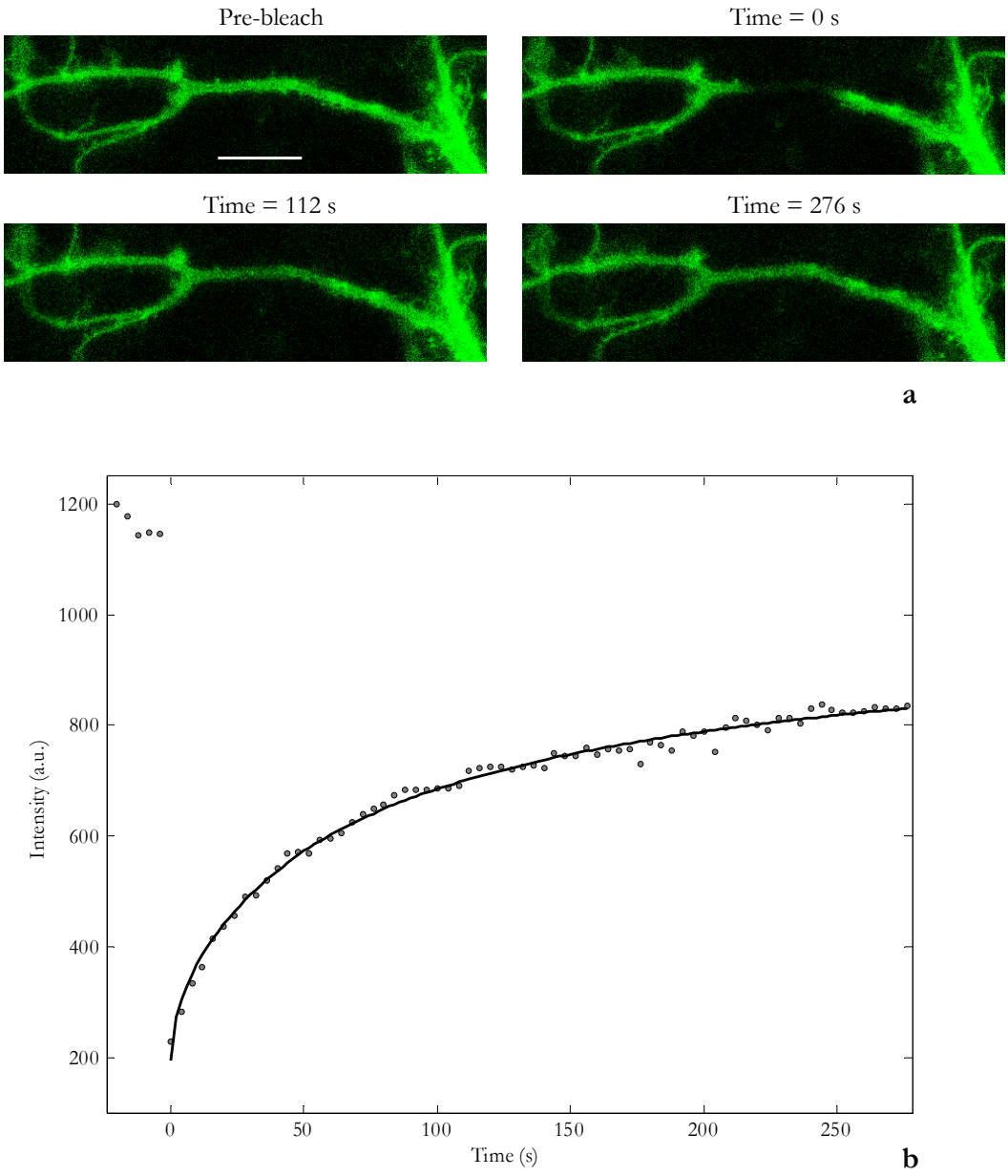

Figure 4.1 (a) Parts of a series of images taken during a FRAP experiment on a dendrite. 0 s is the time directly after bleach and 112 s is the half time of recovery. The scale bar is 10 μm long. (b) The measured FRAP data corresponding to (a) is compared to a fitted, theoretical curve given by Equation (3.7). For this data set, Equation (3.8) and the half time of recovery give a diffusion coefficient of 0.197 $\mu m^2/s$, while curve fitting results in a diffusion coefficient of 0.277 $\mu m^2/s$.

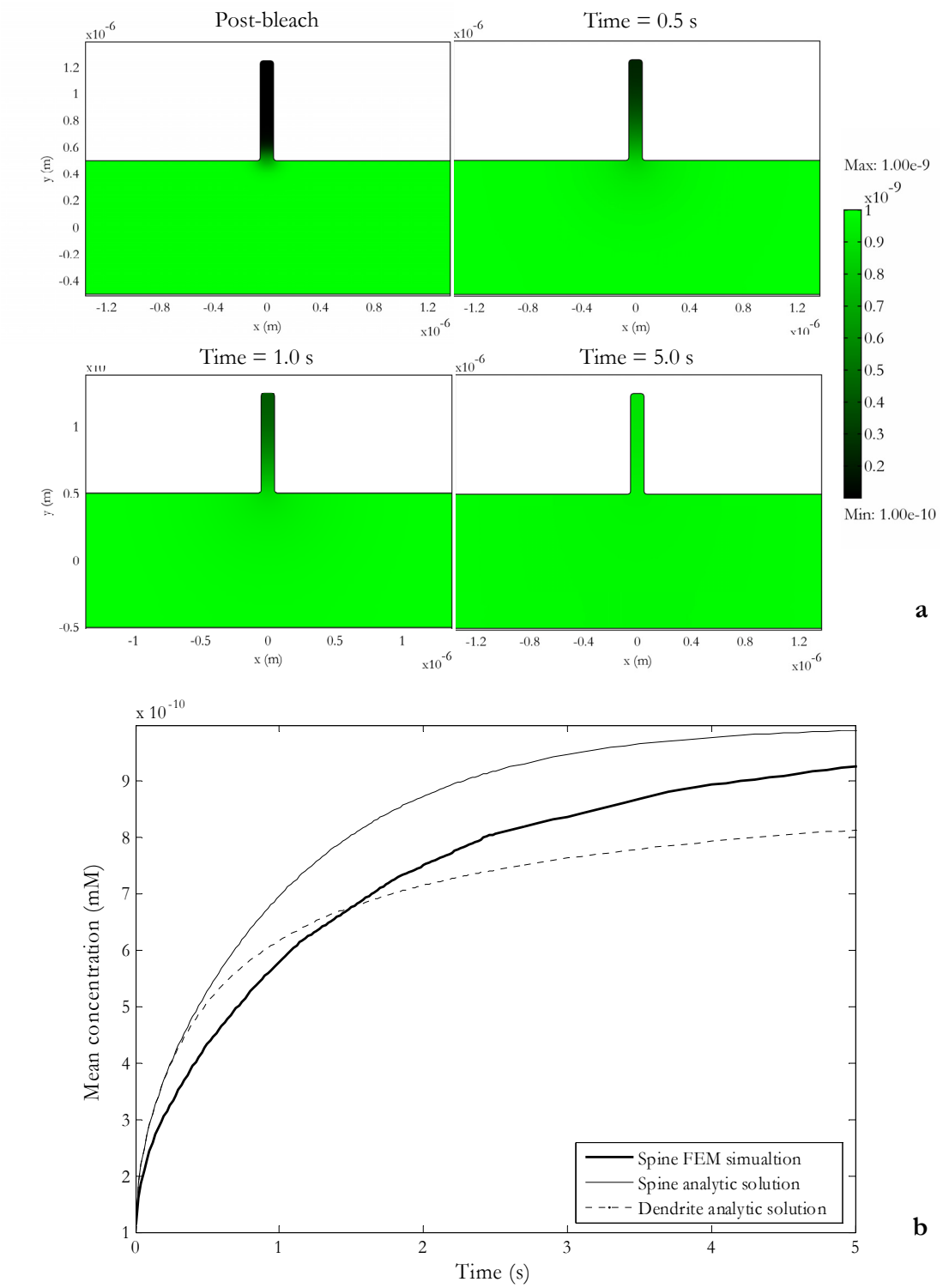

Figure 4.2 (a) Fluorescent recovery in a simulated spine using COMSOL Multiphysics. The color scale indicates concentration of fluorophores in mM. (b) The recovery curves of the two models of diffusion in spines. The thick line shows a recovery curve in a simulated FRAP experiment calculated by numerically integrating a FEM solution to the problem. The thin line shows an analytic solution to the one dimensional spine model. The dashed line is the analytical model of a dendrite with a bleached region with the same length as the spine. The parameters are set as $D = 0.2\ \mu m^2/s$ and $l = 0.375\ \mu m$.

4.1.2 Diffusion transports D1R to active spines

The system of combined diffusion and a reaction trapping fluorescent material as given by Equations (3.15) and (3.16) was simulated using COMSOL Multiphysics. Figure 4.3 shows a simulated FRAP experiment on a dendritic spine. The recovery curve is compared to an increase of fluorescent concentration given by the trapping reaction where the initial condition is homogeneous concentration. By varying the diffusion coefficients, D_1 and D_2, the simulations show that when the bound receptor diffuses more slowly than the unbound, the D1R gets trapped in the spine. If D_1 and D_2 instead are equal, then there is no trapping in the spine; the D1R concentration is thus homogeneous.

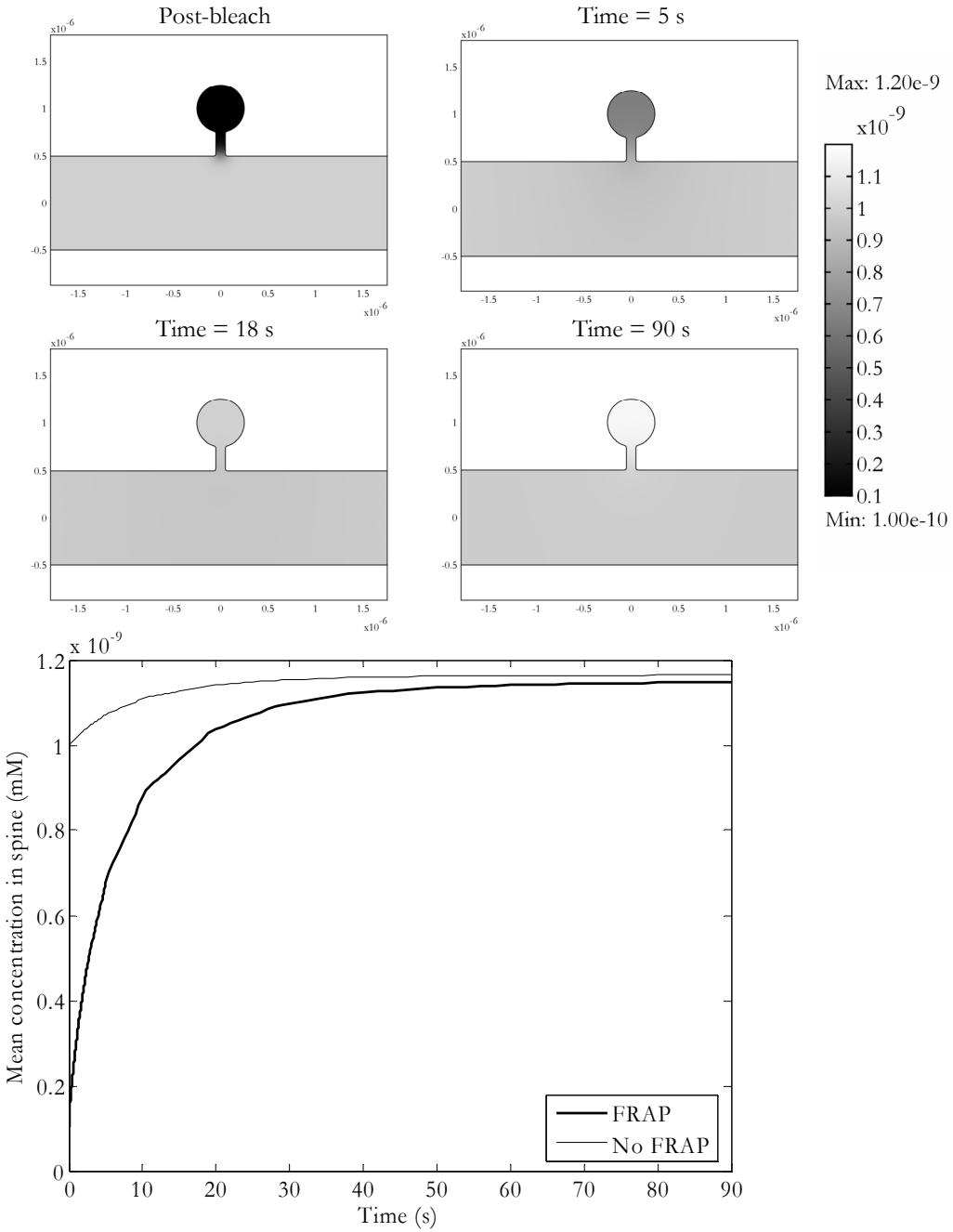

Figure 4.3 A simulated reaction traps diffusing D1R in a spine. The images show a sequence of time frames following initial bleach. After 18 s, fluorescence has recovered fully. The trapping reaction increases the intensity further. The thick curve shows recovery after bleaching while the thin curve shows increase of fluorescence by the trapping reaction alone. The diffusion coefficients are 0.2 $\mu m^2/s$ for the non-trapped substance and five times (0.04 $\mu m^2/s$) smaller for the trapped substance.

4.2 The impact of store-operated calcium entry calcium oscillations

In the Ca^{2+} signaling model in Paper II Ca^{2+} oscillations appear mainly as a cyclic exchange of Ca^{2+} between the ER and cytosol. The cause of these oscillations is stimulation of the IP_3R. In the model, this is controlled by changing the parameter $[IP_3]_{max}$. This parameter determines the maximum IP_3 concentration and can be viewed as the strength of an extracellular signal. Figure 4.4 shows the cyclic movement of Ca^{2+} between the two intracellular regions.

4.2.1 Comparing two models of the IP_3 receptor

The two different models of the IP_3R show strikingly different Ca^{2+} oscillations properties, see Fig. 3 and 6 in Paper II. Mainly the DeYoung and Keizer model that is given by Equation (3.28) results in Ca^{2+} oscillations with lower amplitude, but higher frequency than the Mak-McBride-Foskett model of the IP_3R, given by Equations (3.29) and (3.30). Also the DeYoung and Keizer model shows Ca^{2+} oscillations only within a narrow range of IP_3 concentrations, while the Mak-McBride-Foskett model results in Ca^{2+} oscillations for all IP_3 concentrations above 12 nM.

As shown in Figs. 4-6 in Paper II Store-operated Ca^{2+} entry (SOC) has a strong effect on Ca^{2+} oscillations. When SOC, as given by Equations (3.31)-(3.34), is excluded from the model Ca^{2+} oscillations appear in a wider range and with other characteristics using

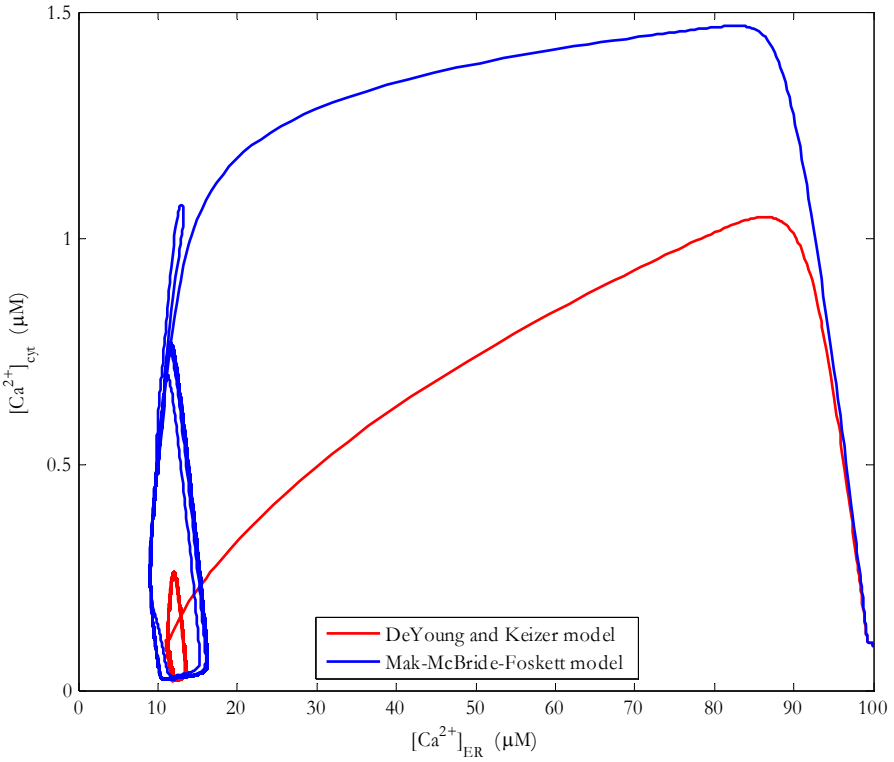

Figure 4.4 Two phase plots showing the cytosolic versus ER Ca^{2+}, corresponding to the two traces in Paper II, Fig. 3. The red curve is based on the De Young and Keizer model of IP_3R and the blue curve on the Mak-McBride-Foskett model. The oscillations appear to the left in the figure, seen as bounded regions where Ca^{2+} is exchanged cyclically between the two compartments. The figure clearly shows the difference in amplitude between the oscillations in the two models, while the period of the oscillations can not be seen.

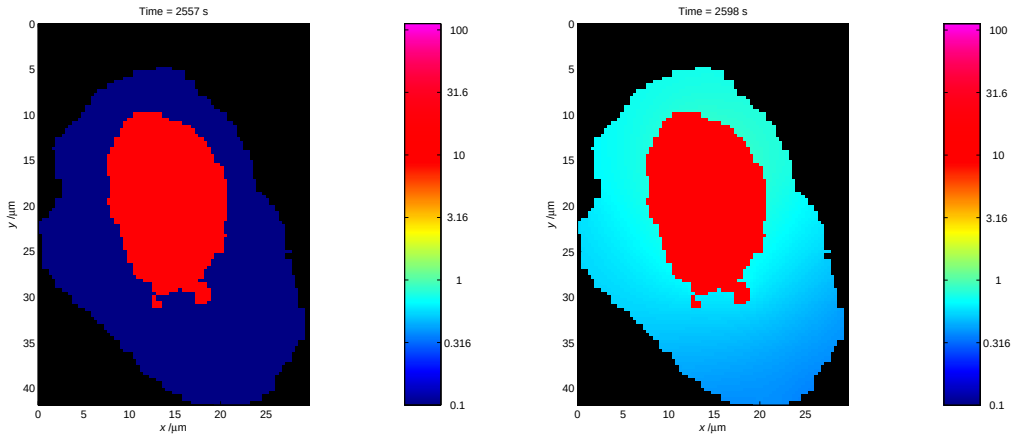

Figure 4.5 The distribution of Ca^{2+} in the modeled cell shown at two points in time. The left panel shows the cells in between two peaks of a Ca^{2+} oscillation while the right panel shows a cell during a peak of cytosolic Ca^{2+} concentration.

the DeYoung and Keizer description compared to the same model where SOC is included. The effect of excluding SOC from the Mak-McBride-Foskett model is an increase in oscillation frequency above a certain level of IP_3 concentration, where the Ca^{2+} flux out of the ER causes a depletion of ER Ca^{2+} which is sufficient to activate SOC channels.

4.2.2 Spatial model

In Paper II a compartmental model of Ca^{2+} signaling and oscillations is presented. A similar spatial model has also been constructed using *Virtual Cell*. The IP_3 dynamics model is simplified compared to the compartmental model and does not depend on Ca^{2+}. However, because IP_3 is produced in the plasma membrane and degraded throughout the cytosol, there will be a stationary distribution of IP_3 in the cell. In an irregular geometry this distribution is non uniform. This causes stimulation of IP_3R that is different in different parts of the ER membrane. The results from this model show similar oscillations compared to the model in Paper II. The oscillations in this model show frequencies around 1 mHz. In the current geometry some regions of the cytosol between the ER and plasma membranes are narrow causing large variation in the peak levels of Ca^{2+} concentration within the cytosol. Between peaks the Ca^{2+} concentration is lower and shows a smaller variation, see Figure 4.5.

Figure 4.6a shows the distribution of cytosolic Ca^{2+} concentrations over time and Figure 4.6b shows the distribution of Ca^{2+} concentration in both ER and cytosol integrated over time. To the left in the figure is a darker area showing the oscillations. The wide upper part of this area represents the bursts of Ca^{2+} which are much more distributed than the lower part representing the time in between bursts. As in Figure 4.4 oscillations appear as a closed curve in the lower left part of the panel.

4.2.3 Geometry dependence

As I have shown earlier [7], narrow regions in a geometry can strongly increase the amplitude of Ca^{2+} transients and oscillations. This is a result of geometry and diffusion and can potentially affect reactions in the cell, such as opening of the IP_3R Ca^{2+} channels.

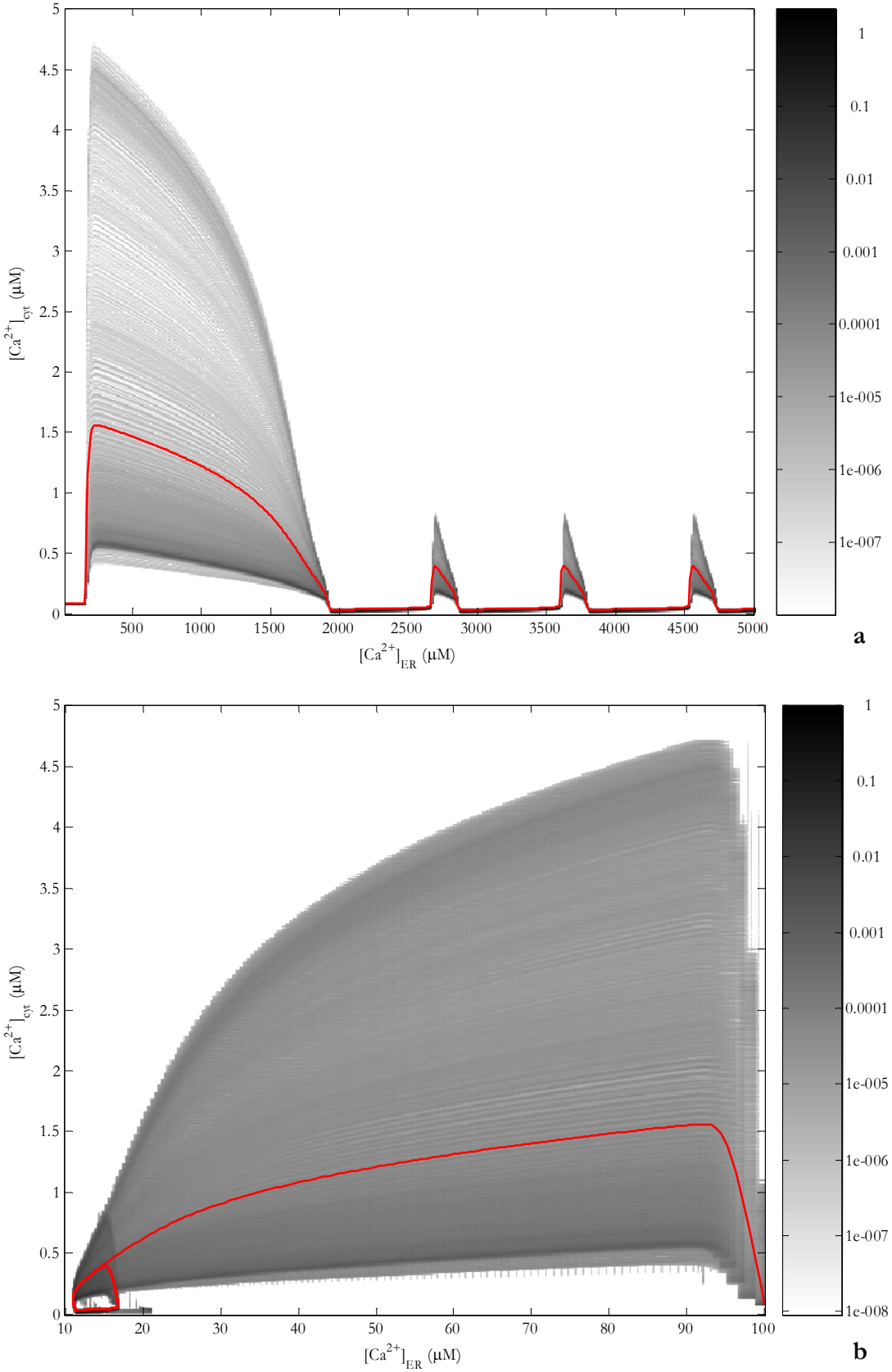

Figure 4.6 (a) Cytosolic Ca^{2+} oscillations in the spatial model. The gray scale shows the distribution of cytosolic Ca^{2+} concentration over time. The red trace shows the mean Ca^{2+} concentration. (b) The same distribution of Ca^{2+} in phase space integrated over time. Dark parts of the diagram indicate that large portions of the cell are in a certain state. Light parts mean that only a small portion of the cell is in that state. The red trace shows the phase plot of the average Ca^{2+} concentration in the two compartments of the cell.

5 Discussion

This thesis presents two projects where mathematical modeling has been used on cellular systems. The results presented are analytical or numerical solutions to equations that can describe these systems according to physical laws of diffusion and reaction rates.

5.1 Methodological limitations

Biological cells display a complexity which has seldom been observed in other systems studied in physics. The large number of interactions in the system requires that any qualitative or quantitative description is greatly simplified. One problem in making quantitative models of biological systems is the lack of good parameter values. In the projects presented in this thesis, parameters have in many occasions been estimated so that steady state occurs in resting systems and that time scales are compatible with experimental results. The complexity in terms of the number of interactions in a system does not necessarily make it unpredictable as the systems are often robust and cooperative [66]. In many cases there exist some key elements which are crucial for the function of a biological system. Identifying these elements may involve both modeling and experiments, calling for a ongoing dialogue between investigators in both these fields.

5.2 Geometrical influence

The models presented in this thesis work with simplified geometrical descriptions of biological cells and detailed analytical and numerical solutions to reaction-diffusion equations. I believe that this approach is sufficient for drawing conclusions about the importance of some geometrical features present in living cells. The focus has been on dendrites and dendritic spines, where the former case represents an almost ideal system for FRAP studies when the diffusion can be assumed to occur only along one axis. In the later case we have shown that the geometry can have a large influence on the recovery profile as seen in a FRAP experiment. An often overlooked fact when measuring diffusion properties of biological systems is the straight forward scaling law of diffusion, which simply states that the time of diffusion across a volume is proportional to the square of the volume's length scale. I believe this to be an important example where basic ideas of physics and biology can merge.

In the Ca^{2+} signaling model the geometrical description showed qualitatively similar results as the compartmental model, however limited diffusion time results in large spatial variations. It has been suggested that thermal fluctuations, as well as fluctuations in concentration caused simply by a low number of particles taking part in reactions can be exploited by cells as a way to switch between different states [67]. As the spatial simulations of Ca^{2+} signaling presented in this thesis show, also a deterministic model can have large variations in concentration if the geometry limits diffusion in certain areas. The results also show that the current system is robust enough to maintain its properties,

in terms of frequency and shape of the Ca^{2+} peaks, even when there are diffusion limited areas.

5.3 Conclusions and future perspectives

The two studies presented in this thesis both deal with biologically relevant questions which have implications in medicine. Mathematical modeling has been used as a tool to build hypotheses that can be compared to experimental results. In both studies the models have resulted in quantitative descriptions of biological systems where the influence of certain parameters can be studied in more detail than was previously possible.

As we have pointed out earlier [2], diffusion can describe the movement of dopamine 1 receptors in dendrites. This study shows that diffusion and trapping reactions fit well to the FRAP experiments that have been performed in Paper I. The numerical simulations described in this thesis show how different geometries can affect the fluorescent recovery and that geometrically constrained reactions can trap diffusing receptors in dendritic spines.

Ca^{2+} signaling and oscillations can be described as a system of contributing channels and pumps leading to slow oscillations in intracellular Ca^{2+}, similar to those observed in experiments. A contributing factor in the oscillating patterns is store-operated Ca^{2+} entry, which affects both qualitative occurrence of oscillations and their characteristics in terms of frequency and amplitude. The system behaves qualitatively similar both when described as a well-stirred compartmental model and as a spatial reaction-diffusion model.

The modeling tools developed during the work on this thesis focus on the spatial and geometrical aspects of cellular biophysics. An area not covered by this thesis, where spatial distribution is of importance, is the role of astrocytes in the brain where substances are transported between intra- and extracellular spaces across several spatial and temporal scales. The characteristics of mathematical modeling are detailed descriptions of dynamic processes. As data from biological experiments increase in resolution and detail, the hypotheses driving the research will have to shift into a more mathematical description.

6 Acknowledgements

Many people have been supportive in the work that has lead to the making of this thesis. I would like to give special attention to some of these people:

My encouraging supervisor Hjalmar Brismar for accepting me as a graduate student, for believing in my possibilities and for his great ideas. A special thank also goes to Anita Aperia who is an amazing person with her vast knowledge, understanding, support and inspiration to all people in the Brismar-Aperia lab. My co-authors: Lena Scott for her skills and true engagement in science, Sergey Zelenin for his knowledge, interest and encouragement, Seth Malmersjö for his humor and wide knowledge in both physics and medicine, Eivor Zettergren-Markus for her expertise and spreading of a good atmosphere around her, Angus C. Nairn and Paul Greengard for good collaboration; Per Uhlén for his help, interest, knowledge, sound skepticism and encouragement; Hiroaki Kitano for inviting me to the Systems biology institute in Tokyo and for his bright ideas.

I would also like to thank my present and former co-workers in the lab: Andreas, Susanna, Gustav, Kanchana, Erland, Victor, Padideh, Linda, Markus, Eli, Marina, Oleg, Ann-Christine, Juan, Ayako, Ulla, Patrik, Tove, Mårten and Raija, for making the days at work a pleasant and inspiring experience. Special thanks go to Rick Rogers and Gerald F. DiBona for their help with manuscript reading and being great sources of inspiration. I would also like to thank Mineo Morohashi, Akira Funahashi and Noriko Hiroi, for showing me around Tokyo, choosing great places for lunch and dinner and making me feel so comfortable at the institute.

Another thank goes to my spare-time friends: Jon, Peter and Josef for always being there for me, for coping with me at all times and for helping me with so many practical things.

Last but not least I would like to thank my parents, Nina and Jozef, for all support, encouragement, trust and good advice; Ulrica, for always being there for me, for support comfort, love and understanding; Eva for being a strong, kind and caring person. I would also like to express the loving memory of my courageous and supporting grandparents.

7 References

1. Weiss, T.F., *Cellular biophysics*. Vol. 1, Transport. 1996: The MIT Press.
2. Scott, L., *Plasticity in the dopamine 1 receptor system: behavior and cell biological studies*, in *Dept. of Woman and Child health*. 2004, Karolinska Institutet: Stockholm. p. 51.
3. Hancock, J.T., *Cell signaling*. 1997, Edinburgh Gate, Harlow, Essex, England: Addison Wesley Longman.
4. Falcke, M., *Reading the patterns in living cells - the physics of Ca2+ signaling*. Adv. Phys., 2004. **53**(3): p. 255-440.
5. Uhlén, P., *Signal Transduction via Ion Fluxes*, in *Department of Woman and Child Health*. 2002, Karolinska Institutet: Stockholm.
6. Huss, M., *Computational models of lamprey locomotor network neurons*, in *Numerical Analysis and Computer Science*. 2005, KTH.
7. Kowalewski, J., *Mathematical modelling of intra-cellular Ca^{2+} signalling*, in *Cell physics*. 2003, Royal Institute of Technology: Stockholm.
8. Sonesson, A., *Lipase diffusion on solid surfaces*, in *Physics*. 2005, Royal Inst. of Technology.
9. Erikson, T. and et al., *Fysikens matematiska metoder*. 1997, Stockholm: Theoretical Physics, KTH.
10. Chudler, E.H. *Brain Facts and Figures*. [cited 2005 November 4, 2005]; Available from: http://www.univ.trieste.it/~brain/NeuroBiol/Neuroscienze%20per%20tutti/facts.html#neuron.
11. Gunnarson, E., et al., *Lead induces increased water permeability in astrocytes expressing aquaporin 4*. Neuroscience, 2005. **136**(1): p. 105.
12. Singer, S.J. and L. Nicolson, *The Fluid Mosaic Model of the Structure of Cell Membranes*. Science, 1972. **175**: p. 720-731.
13. Poo, M.-m., *Mobility and Localization of Proteins in Excitable Membranes*. Annual Review of Neuroscience, 1985. **8**(1): p. 369-406.
14. Frye, L.D. and M. Edidin, *The Rapid Intermixing of Cell Surface Antigens After Formation of Mouse-Human Heterokaryons*. J Cell Sci, 1970. **7**(2): p. 319-335.
15. Axelrod, D., et al., *Mobility measurement by analysis of fluorescence photobleaching recovery kinetics*. Biophys. J., 1976. **16**(9): p. 1055-1069.
16. Despopoulos, A. and S. Silbernagl, *Color atlas of physiology*. 5th ed. 2003, Stuttgart: Thieme.
17. Alberts, B., et al., *Molecular biology of the cell*. 2002: Garland Publising.
18. Alberts, B., et al., *Essential cell biology*. 2nd ed. 2004, New York: Galand Science Taylor & Francis Group.
19. Wikipedia. *Signal transduction - Wikipedia,The Free Encyclopedia*. 2006 [cited March 22nd 2006]; Available from: http://en.wikipedia.org/w/index.php?title=Signal_transduction&oldid=43146521.
20. Stryer, L., *Biochemistry*. 1999: W. H. Freeman and Company.
21. Fall, C.P., et al., eds. *Computational Cell Biology*. 2002, Springer-Verlag: New York.
22. Weiss, T.F., *Cellular biophysics*. Vol. 2, Electrical properties. 1996: The MIT Press.
23. Nauli, S.M. and J. Zhou, *Polycystins and mechanosensation in renal and nodal cilia*. BioEssays, 2004. **26**: p. 844-856.
24. Putney, J.W., Jr., ed. *Calcium signaling*. Methods in signal transduction. 2000, CRC Press: Boca Raton, Florida.
25. Berridge, M.J., *Inositol trisphosphate and calcium signalling*. Nature, 1993. **361**(6410): p. 315.

26. Bezprozvanny, I., J. Watras, and B.E. Ehrlich, *Bell-shaped calcium-response curves of lns(1,4,5)P3- and calcium-gated channels from endoplasmic reticulum of cerebellum.* Nature, 1991. **351**: p. 751-754.
27. Taylor, C.W., *Inositol trisphosphate receptors: Ca2+-modulated intracellular Ca2+ channels.* Biochimica et Biophysica Acta (BBA) - Molecular and Cell Biology of Lipids, 1998. **1436**(1-2): p. 19.
28. Hagar, R.E., et al., *Type III InsP3 receptor channel stays open in the presence of increased calcium.* Nature, 1998. **396**: p. 81-84.
29. Ramos-Franco, J., M. Fill, and G.A. Mignery, *Isoform-specific function of single inositol 1,4,5-trisphosphate receptor channels.* Biophys. J., 1998. **75**: p. 834-839.
30. Missiaen, L., et al., *Functional Properties of the Type-3 InsP3 Receptor in 16HBE14o- Bronchial Mucosal Cells.* J. Biol. Chem., 1998. **273**(15): p. 8983-8986.
31. Hattori, M., et al., *Distinct Roles of Inositol 1,4,5-Trisphosphate Receptor Types 1 and 3 in Ca^{2+} Signaling.* J. Biol. Chem., 2004. **279**(12): p. 11967-11975.
32. Miyakawa-Naito, A., et al., *Cell signaling microdomain with Na,K-ATPase and inositol 1,4,5-trisphosphate receptor generates calcium oscillations.* J Biol Chem, 2003. **278**(50): p. 50355-61.
33. Mak, D.-O.D., S. McBride, and J.K. Foskett, *Inositol 1,4,5-tris-phosphate activation of inositol tris-phosphate receptor Ca2+ channel by ligand tuning of Ca2+ inhibition.* PNAS, 1998. **95**(26): p. 15821-15825.
34. De Young, G.W. and J. Keizer, *A Single-Pool Inositol 1,4,5-Trisphosphate-Receptor-Based Model for Agonist-Stimulated Oscillations in Ca2+ Concentration.* PNAS, 1992. **89**(20): p. 9895-9899.
35. Mikoshiba, K. and M. Hattori, *IP_3 Receptor-Operated Calcium Entry.* Science's STKE, 2000. **2000**(51): p. 1.
36. Sneyd, J., et al., *A dynamic model of the type-2 inositol trisphosphate receptor.* PNAS, 2002. **99**(4): p. 2398-2403.
37. Sneyd, J. and M. Falcke, *Models of the inositol trisphosphate receptor.* Progress in Biophysics and Molecular Biology, 2005. **89**(3): p. 207-245.
38. Parekh, A.B. and J.W. Putney, Jr., *Store-Operated Calcium Channels.* Physiol. Rev., 2005. **85**(2): p. 757-810.
39. Putney, J.W., Jr, *A model for receptor-regualated calcium entry.* Cell Calcium, 1986. **7**: p. 1-12.
40. Hoth, M. and R. Penner, *Depletion of intracellular calcium stores activates a calcium current in mast cells.* Nature, 1992. **355**(6358): p. 353.
41. Parekh, A.B., *Store-operated Ca2+ entry: dynamic interplay between endoplasmic reticulum, mitochondria and plasma membrane.* Journal of Physiology, 2003. **547**(2): p. 333-348.
42. Randriamampita, C. and R.Y. Tsien, *Emptying of intracellular Ca2+ stores releases a novel small messenger that stimulates Ca2+ influx.* Nature, 1993. **364**(6440): p. 809.
43. Ma, H.-T., et al., *Requirement of the Inositol Trisphosphate Receptor for Activation of Store-Operated Ca2+ Channels.* Science, 2000. **287**(5458): p. 1647-1651.
44. Venkatachalam, K., et al., *The cellular and molecular basis of store-operated calcium entry.* Nature Cell Biol., 2002. **4**(11): p. 263-272.
45. Aizman, O., et al., *Ouabain, a steroid hormone that signals with slow calcium oscillations.* PNAS, 2001. **98**(23): p. 13420-13424.
46. Uhlén, P., et al., *α-Haemolysin of uropathogenic E. coli induces Ca2+ oscillations in renal epithelial cells.* Nature, 2000. **405**: p. 694-697.
47. Berridge, M.J., M.D. Bootman, and P. Lipp, *The versatility and universality of calcium signalling.* Nature Reviews. Molecular Cell Biology, 2000. **1**: p. 11-21.
48. Tang, Y. and H.G. Othmer, *Frequency encoding in excitable systems with applications to calcium oscillations.* PNAS, 1995. **92**: p. 7869-7873.
49. Sneyd, J., ed. *Tutorials in mathematical biosciences. 2, Mathematical modeling of calcium dynamics and signal transduction.* Lecture notes in mathematics. Vol. 1867. 2005, Springer: Berlin.
50. De Koninck, P. and H. Schulman, *Sensitivity of CaM Kinase II to the Frequency of Ca2+ Oscillations.* Science, 1998. **279**(5348): p. 227-230.
51. Baker, H.L., et al., *A Mathematical Model Predicts that Calreticulin Interacts with the Endoplasmic Reticulum Ca2+-ATPase.* Biophys. J., 2002. **82**(2): p. 582-590.

52. Hallén, K., et al., *mGluR-Mediated calcium oscillations in the lamprey: a computational model.* Neurocomputing, 2004. **58-60**: p. 431-435.
53. Fink, C.C., B. Slepchenko, and L.M. Loew, *Determination of Time-Dependent Inositol-1,4,5-Trisphosphate Concentrations during Calcium Release in a Smooth Muscle Cell.* Biophys. J., 1999. **77**(1): p. 617-628.
54. Slepchenko, B.M., et al., *Computational Cell Biology: Spatiotemporal Simulation of Cellular Events.* Annu. Rev. Biophys. Biomol. Struct., 2002. **31**(1): p. 423-441.
55. Fink, C.C., et al., *An Image-Based Model of Calcium Waves in Differentiated Neuroblastoma Cells.* Biophys. J., 2000. **79**(1): p. 163-183.
56. Westermark, P., *Physical biochemistry*. 2002.
57. Kummer, U., et al., *Switching from Simple to Complex Oscillations in Calcium Signaling.* Biophys. J., 2000. **79**(3): p. 1188-1195.
58. Goldbeter, A., *Computational approaches to cellular rhythms.* Nature, 2002. **420**(6912): p. 238-245.
59. *The Matlab documentation*. 2003 [cited 2005 May]; Available from: http://www.mathworks.com/access/helpdesk/help/techdoc/matlab.html.
60. Shampine, L.F. and M.W. Reichelt. *The Matlab ODE suite.* [cited 2006 February 7]; Available from: http://www.mathworks.com/access/helpdesk/help/pdf_doc/otherdocs/ode_suite.pdf.
61. Heath, M.T., *Scientific computing: an introductory survey*. Computer science series. 1996, Singapore: McGraw-Hill.
62. Schaff, J., et al. *The Virtual Cell Portal.* [cited 2005 May]; Available from: http://www.vcell.org.
63. Kruse, M.S., et al., *Recruitment of renal dopamine 1 receptors requires an intact microtubulin network.* Pflugers Arch, 2003. **445**(5): p. 534-9.
64. Scott, L., et al., *Selective up-regulation of dopamine D1 receptors in dendritic spines by NMDA receptor activation.* Proc Natl Acad Sci U S A, 2002. **99**(3): p. 1661-4.
65. Uhlén, P., *Spectral analysis of calcium oscillations.* Sci STKE, 2004. **2004**(258): p. pl15.
66. Kitano, H., *Computational systems biology.* Nature, 2002. **420**: p. 206-210.
67. Rao, C.V., D.M. Wolf, and A.P. Arkin, *Control, exploitation and tolerance of intracellular noise.* Nature, 2002. **420**(6912): p. 231.

Appendix A: Object Oriented Reaction toolbox documentation

Object Oriented Reaction toolbox (*OOR toolbox*) is a MATLAB® toolbox for creating and simulating chemical reactions involving one or more compartments. Models are built up by species localized in compartments. Reactions connect the species by describing them as reactants, product or catalysts. *OOR toolbox* is fully integrated, and created in MATLAB®, making it possible to automate changing of model properties such as reaction pathways and parameter values from a MATLAB® script or the command line interface. The structure of models built in *OOR toolbox* is similar to the structure of *The Systems Biology Markup Language* (SBML) [1, 2]. *OOR toolbox* uses MATLAB® m-functions, as well as anonymous and inline functions, to define rules. This makes it possible to construct more general models than are easily created using SBML. At this time *OOR toolbox* is not compatible with SBML. The interested reader may see the SBML toolbox for MATLAB® [3] which can import, manipulate and simulate SBML models in MATLAB®.

A model is created in *OOR toolbox* using the object oriented command line interface in MATLAB®. A model is an object containing several other objects such as compartments, species, and reactions. These objects are created and combined using special m-functions called methods. A method is a function working on an object. Methods are defined for a certain class, a type definition and description of that type of objects [4].

A.1 Object structure

The classes in *OOR toolbox* are **`model`**, **`comp`** (compartment), **`species`**, **`reaction`**, **`transport`** (a subtype of reaction), and **`speciesref`** (reference to a species object). The transport object works similarly to flux reactions in *Virtual Cell* [5]. Each class has methods which can be called from within MATLAB® as long as the OOR directory is in the search path. Observe: The class directories do not have to be added to the search path. A special method is the constructor which has the same name as the class; it is used to define a new object of that class.

The most fundamental object in *OOR toolbox* is a **`model`**. In most cases modeling in *OOR toolbox* begins with a call to the **`model`** constructor. Other objects such as compartments, species and reactions are added to a model using the **`add`** method, see below. The model object contains all other objects used in the calculation. Species and reactions added to a model are automatically numbered and can be referred to by number. Compartments are not number, and are only possible to refer to by name. Species can be referred to either by number or hierarchically in the form **`model.compartment.species`**. Reactions describe dynamical properties of the model and connect species by containing references to them either as reactants, products or catalysts. Reactions contain function handles or inline objects that express the rate of conversion from reactants to products as a function of the concentration of each species referred to by the reaction object. Reaction rates can also depend on a number of parameters contained in the model. The structure of an *OOR toolbox* model follows similar principles as those described by the SBML definition [2].

A.1.1 Simulations

A model can in principle describe different kinds of dynamics, not necessarily by compartmental models and ordinary differential equations (ODEs). *OOR toolbox* takes advantage of the flexible type definitions in MATLAB® so that a species concentration can be either a scalar, to express its initial amount, a vector, to express a time series, or an array of any number of dimensions to express e.g. a spatial dependence. Presently the only implemented kind of simulation is an interface to MATLAB®'s ODE solvers. This interface is the **`odesim`** method in the **`model`** class. It simulates the dynamics of a model expressing it as a system of ODEs, see below. The output of **`odesim`** is a new model object containing the same species and reaction objects as before but with species concentrations replaced by the times series corresponding to the numerical solution to the system of ODEs.

A.2 Class definitions

A.1.2 Model class

Constructor

`model(mod)`
constructs a new empty model object or uses the persistent one if it exists. If the argument mod is specified, the new model is a copy.

Methods

`add(mod,comp)`
adds a compartment to a model **`mod`**.

`add(mod,spec)`
adds a species **`spec`** to a model **`mod`**. The species **`spec`** is added to its compartment. If it has not yet been assigned a number, this function does that. An already numbered **`spec`** replaces an old species with that number. A species with a name and compartment already present in **`mod`** replaces the old species with the same name and compartment.

`add(mod,reaction)`
adds a reaction to a model.

`add(mod,params)`
adds parameters to **`mod`** contained in the structure **`params`**.

`str = char(mod)`
converts **`mod`** to string **`str`** containg detailed information about the model.

`N = getcouplings(mod)`
returns the couplings matrix of the model mod. It differs from the stoichiometry matrix in the way that it includes information on compartment sizes in transport reactions.

spec = getspecies(mod,n)
gets species from a model. Returns species **n** (1 or more if **n** is non-scalar) from the model. If **n** is not assigned, all species are returned.

N = getstoich(mod)
returns the stoichiometry matrix of the model **mod**. The size of **N** is (the number of species) × (the number of reactions) in **mod**.

odesim(mod,time,odesolver)
simulates a model during the time span **time**, using **odesolver**. If **time** is scalar and **time** is within the time span of **mod.time**, a model which is equal to **mod** at a time close to **time** will be returned. If **odesolver** is not specified **ode15s** is selected.

h = plot(mod,x,varargin)
plots species concentrations or flux rates in a model. **x** is either a species, a flux or the string **'time'**. The following arguments can be species, species references, or reactions. The returned value **h** is a handle to graphics objects as in the built in **plot** function. If **x** is not specified, all concentrations will be plotted as functions of time.

x = subsref(A,s)
returns a species object when called as **A.<compartmentname>.<speciesname>**. Called as **A.<compartmentname>** this method returns a compartment object. In other cases this method returns any field from a model **A**. E.g. **A.params** returns a structure of parameters and **A.time** returns the time vector of **A**.

A.1.3 Compartment class

Constructor

comp(name,size,outside,dim,varargin)
defines a new **comp** object. **name** is a string, **size** is a number, and **dim** is an integer describing the number of dimension of the new compartment.

Methods

addspec(c,spec)
adds a species to a compartment. The species **spec** is added to **c**. This method is mainly used by the **add(species)** method in the model class.

str = char(c)
returns the name of **c**.

setspecies(c,spec)
sets the species reference vector of a compartment to **spec**.

A.1.4 Species class

Constructor

species(name,comp,conc,charge,unit,varargin)
defines a species object. A species has a name, a compartment, a concentration, a charge and a concentration unit. To have the same species in several compartments, a

list of compartments can be given with corresponding concentrations. The name is compulsory, the rest can be set to default values.

Methods

`str = char(s,format)`
converts the species **`s`** to a charater string **`str`**. If the concentration is an array it will be displayed as the size and type of data. **`format`** can be one of **`'long'`**, **`'short'`** **`'context'`** and **`'conc'`**. **`'long'`** is the default.

`display(s)`
prints **`char(s)`** in the command window.

`n = getnumber(spec)`
returns the numbers of spec as a vector.

`[mtimes] specref = n*species`
returns a speciesref **`specref`** where the stoichiometry is multiplied by **`n`**.

`[plus] specref = s1 +s2`
creates a speciesref merged from **`spec1`** and **`spec2`**. Equal references are summed. This is a kind of algebraic sum intended for stoichiometry modeling.

`setconc(s,c)`
sets the concentration of a species **`s`** to **`c`**.

`setnumber(s,n)`
sets the number of a species **`s`** to **`n`**.

A.1.5 Species reference class

Constructor

`speciesref(s,n)`
constructs a **`speciesref`** object. **`s`** can be a species vector, **`speciesref`** or a $N\times2$ matrix containing species numbers in the first and stoichiometries in the second column. The stoichiometry vector **`n`** is set to 1 by default and may be excluded.

Methods

`str = char(s,format,mod)`
converts **`s`** to string **`str`** using format. See also **`species/char`**.

`[mtimes] specref = n*spesref`
creates a species reference where the stoichiometry is multiplied by **`n`**.

`[plus] specref = specref1 + specref2`
creates **`specref`** merged from **`specref1`** and **`specref2`**. Equal references are summed. This is a kind of algebraic sum intended for stoichiometry modeling.

A.1.6 Reaction class

Constructor

`reaction(rule,reactants,products,catalysts,varargin)`
constructs a reaction object that can be added to a model. **`rule`** is a function handle, **`reactants`**, **`products`** and **`catalysts`** are species or species references. Additional arguments should be strings containing names of the parameters for the reaction object.

Methods

`str = char(r)`
returns the name of **`r`**.

`str = char(r,mod)`
converts **`r`** to a longer string containing information about the references from **`r`** to the model **`mod`**.

`display(r)`
prints **`char(r)`** in the command window.

`setnumber(r,n)`
sets the number of a reaction **`r`** to **`n`**.

`setrule(r,rule)`
sets the rule of a reaction **`r`** to **`rule`**.

`subsref(r,x)`
returns a vector **`rate`** containing the flux by **`r`** at every time in **`x.time`** when called as **`rate = r(x),`** where **`x`** is a **`model`**. Otherwise this is a general **`subsref`** method which returns any field name **`x`** from the reaction **`r`**.

A.1.7 Transport class

Constructor: `transport(rule,comp1,comp2,specs,varargin)`

creates a transport reaction involving species **`specs`** going from compartment **`comp1`** to **`comp2`**. **`transport`** is a subclass of **`reaction`**. Additional arguments are strings containing names of the parameters for the transport object.

Method: `setcomps(t,comp1,comp2)`

sets the compartments of **`t`** to **`comp1`** and **`comp2`**.

A.3 Example: Ca^{2+} signaling model

Below follows a MATLAB® script and some functions that together use the *OOR toolbox* to create the Ca^{2+} signaling model presented in Paper II.

A.1.8 Script

```
% CA_SIGNALING script defines the model object.
% Creates a model and runs a Matlab simulation of intracellular
% Ca-signaling.
%
% Jacob Kowalewski 2006

clear setmodel params SOCt Cell
Cell_ID = length(dir('Cell*.mat'))+1

OORpath = pwd;
OORpath = [OORpath(1:length(OORpath)-6) 'OOR']
addpath(OORpath);

tic
params.X=0.4;
params.Y=0.6;
params.r1=0.185;

params.v2=0.002;
params.V_IP3R=0.7*0.1;
params.K_inf=52;
params.IP3R_actCa=210E-3;
params.K_IP3=50E-3;

params.d1=0.13;
params.d2=0.5;
params.d3=9.4E-3;
params.d5=82.34E-3;
params.v1=10;

params.VmaxPMCA=0.245*0.6;
params.VmaxSERCA=0.95*2;
params.K05=0.2;
params.K05_SERCA=0.5;
params.V_SOC=5E-3;
params.leak_PM=1.2E-5;

params.I_deg=0.01;
params.I_R=0.01;
params.period_IP3=5000;
params.T_IP3prod=3000;
params.IP3max= 40E-3

params.k_G=0.2;
params.G_max=1;
params.G_deg=0.5;

params.kZ=2e-4;
params.Zmax=0.1;
params.kSOC=1.7;
params.I_SOC=0.002;
params.Ca_ER_min=10;
params.vZ=1

Cell = model;
Cell = add(Cell,params);
```

```
Cell = add(Cell,comp('EC',inf));
Cell = add(Cell,comp('PM',1/params.r1,'EC'));
Cell = add(Cell,comp('cyt',1/params.r1,'PM'));
Cell = add(Cell,comp('ER',1,'cyt'));

% Initial conditions

Cell = add(Cell,species('Ca',{'cyt','ER','EC'},{0.095,100,10000*0.095},2));
Cell = add(Cell,species('IP_3',Cell.cyt,1E-9,0));
Cell = add(Cell,species('G',Cell.cyt,0));
Cell = add(Cell,species('Z',{'cyt','ER'},{0,0.1}));
Cell = add(Cell,species('SOC','PM',0));

% Reactions
r_SERCA =
transport(@SERCA,Cell.cyt.Ca,Cell.ER.Ca,[],'VmaxSERCA','K05_SERCA','Y');

r_PMCA = transport(@PMCA,Cell.EC.Ca,Cell.cyt.Ca,[],'VmaxPMCA','X','K05');

r_IP3RMak = transport(@IP3RMak,Cell.cyt.Ca,Cell.ER.Ca,Cell.cyt.IP_3,'v2',
...
                      'V_IP3R','K_inf','IP3R_actCa','K_IP3');
r_IP3R = transport(@IP3R,Cell.cyt.Ca,Cell.ER.Ca,Cell.cyt.IP_3, ...
                'v2','d1','d2','d3','d5','v1');
r_SOC = transport(@SOC,Cell.EC,Cell.cyt,'Ca',Cell.PM.SOC, ...
                      'V_SOC','leak_PM');
r_RyR = transport(@RyR,Cell.ER.Ca,Cell.cyt.Ca,[],'vRyR','Ka','Kb', ...
               'Kc');

Grule = inline('k_G*Ca - G_deg*G','G','Ca','k_G','G_deg','t')
IP3rule = inline('G_signal_loop(t,G,G_max).*IP3max*I_deg -
I_deg*IP3','IP3','G','IP3max','I_deg','G_max','t')

Cell = add(Cell,r_PMCA);
Cell = add(Cell,r_SERCA);
Cell = add(Cell,r_IP3R);
%Cell = add(Cell,r_IP3RMak);
Cell = add(Cell,r_SOC);

Cell = add(Cell,reaction(Grule,[],Cell.cyt.G,Cell.cyt.Ca,'k_G','G_deg'));
Cell =
add(Cell,reaction(IP3rule,[],Cell.cyt.IP_3,Cell.cyt.G,'IP3max','I_deg','G_ma
x'));

Cell = add(Cell,reaction(@Zprod,[],Cell.ER.Z,[],'kZ','Zmax'));
Cell = add(Cell,transport(@SOCbind,Cell.cyt.Z,Cell.PM.SOC,[],'kSOC'));
Cell = add(Cell,reaction(@SOCdegrad,Cell.PM.SOC,[],[],'I_SOC'));
Cell = add(Cell,transport(@Ztransp,Cell.ER,Cell.cyt,'Z', ...
                      Cell.ER.Ca,'Ca_ER_min','vZ'));

% Simulate the whole thing
Cell = setmodel(Cell);
spec=getSpecies(model)

Cell=odesim(Cell,[0 7000],@ode15s)
filename = ['Cell_' num2str(Cell_ID)]
figure(1)
plot(Cell,'t',Cell.cyt.Ca,Cell.cyt.IP_3)
save(filename,'Cell');
```

A.1.9 Functions describing the transporters

```
function signal=G_signal_loop(t,G,G_max)
n=1;
signal=(t>500)*G_max*(1-Hill(G,n,G_max/2));

function flux=Hill(c,n,c_05)
% Hill-type flux equation

flux=c.^n./(c.^n + c_05^n);
function J=IP3R(CaCyt,CaER,IP3,v2,d1,d2,d3,d5,v1,t)
%global v2 V_IP3R K_inf IP3R_actCa K_IP3 d1 d2 d3 d5 v1;
%J=-(CaER-CaCyt)*(v2+v1*(d2*IP3*exp(-((CaCyt-0.6)/0.2)^2)));

%H_inh=4;
%H_act=2;
%H_IP3=4;
%IP3R_inhCa=K_inf./(1 + (K_IP3./IP3).^H_IP3);
%J=-(CaER-CaCyt).*(v2 + V_IP3R./((1 + (IP3R_actCa./CaCyt).^H_act) .* ...
%                            (1 + (CaCyt./IP3R_inhCa).^H_inh)));
J=-(CaER-CaCyt).*(v1*(CaCyt.*IP3*d2./((CaCyt.*IP3 + IP3*d2+d1*d2 +
CaCyt*d3).*(CaCyt+d5))).^3+v2);

function J=PMCA(CaEC,CaCyt,VmaxPMCA,X,K05,t)
n=2;
J=-X*VmaxPMCA.*CaCyt.^n./(CaCyt.^n+K05^n);

function J=SERCA(CaCyt,CaER,VmaxSERCA,K05_SERCA,Y,t)
n=1;
blocked_range = (t<100000|t>200000);
J=Y*VmaxSERCA*(0+1*blocked_range).*CaCyt.^n./(CaCyt.^n+K05_SERCA^n);

function J=SOC(CaEC,CaCyt,SOC,V_SOC,leak_PM,t)

J = (V_SOC*SOC + leak_PM) .* (CaEC-CaCyt);
%SOC_flag=~isempty(indexOn);
%tSOC=[tSOC;t];
%JSOC=[JSOC;J];


function J = SOCbind(Z_cyt,SOC_PM,kSOC,t)
J= kSOC*Z_cyt;

function J = SOCdegrad(SOC_PM,I_SOC,t)
J= I_SOC*SOC_PM;

function J = Zprod(Z_ER,kZ,Zmax,t)
J= kZ*(Zmax-Z_ER);

function J = Ztransp(Z_ER,Z_cyt,Ca_ER,Ca_ER_min,vZ,t)
J= (Ca_ER<Ca_ER_min)*vZ.*(Z_ER - Z_cyt);
```

Time = 0
Species:
$[Ca^{2+}]_{cyt}$ = 0.095µM (1)
$[Ca^{2+}]_{ER}$ = 100µM (2)
$[Ca^{2+}]_{EC}$ = 950µM (3)
$[IP_3]_{cyt}$ = 1e−09µM (4)
$[G]_{cyt}$ = 0µM (5)
$[Z]_{cyt}$ = 0µM (6)
$[Z]_{ER}$ = 0.1µM (7)
$[SOC]_{PM}$ = 0µM (8)

Reactions:
$Ca^{2+}_{cyt} \rightarrow Ca^{2+}_{EC}$ (VmaxPMCA,X,K05): PMCA (1)
$Ca^{2+}_{cyt} \rightarrow Ca^{2+}_{ER}$ (VmaxSERCA,K05_ERCA,Y): SERCA (2)
$Ca^{2+}_{cyt} \rightarrow Ca^{2+}_{ER}$ (IP_{3cyt},v2,V_IP3R,$K_i$nf,IP3R_ctCa,K_IP3): IP3RMak (3)
$Ca^{2+}_{EC} \rightarrow Ca^{2+}_{cyt}$ (SOC_{PM},V_SOC,$leak_P$M): SOC (4)
$\rightarrow G_{cyt}$ (Ca^{2+}_{cyt},k_G,$G_d$eg): Grule (5)
$\rightarrow IP_{3cyt}$ (G_{cyt},IP3max,$I_d$eg,$G_m$ax): IP3rule (6)
$\rightarrow Z_{ER}$ (kZ,Zmax): Zprod (7)
$Z_{cyt} \rightarrow SOC_{PM}$ (kSOC): SOCbind (8)
$SOC_{PM} \rightarrow$ (I_SOC): SOCdegrad (9)
$Z_{ER} \rightarrow Z_{cyt}$ (Ca^{2+}_{ER},$Ca_E R_m$in,vZ): Ztransp (10)

X = 0.4
Y = 0.6
r1 = 0.185
v2 = 0.002
V_IP3R = 0.07
$K_i$nf = 52
IP3R_ctCa = 0.21
K_IP3 = 0.05
d1 = 0.13
d2 = 0.5
d3 = 0.0094
d5 = 0.08234
v1 = 10
VmaxPMCA = 0.147
VmaxSERCA = 1.9
K05 = 0.2
$K05_S$ERCA = 0.5
V_SOC = 0.005
$leak_P$M = 1.2e−05
$I_d$eg = 0.01
I_R = 0.01
$period_I$P3 = 5000
T_IP3prod = 3000
IP3max = 4e−05
k_G = 0.2
$G_m$ax = 1
$G_d$eg = 0.5
kZ = 0.0002
Zmax = 0.1
kSOC = 1.7
I_SOC = 0.002
$Ca_E R_m$in = 10
vZ = 1

Figure A.1 Example of output from `char(Cell)` in a Matlab® figure. This shows a summary of the model made by the MATLAB® script.

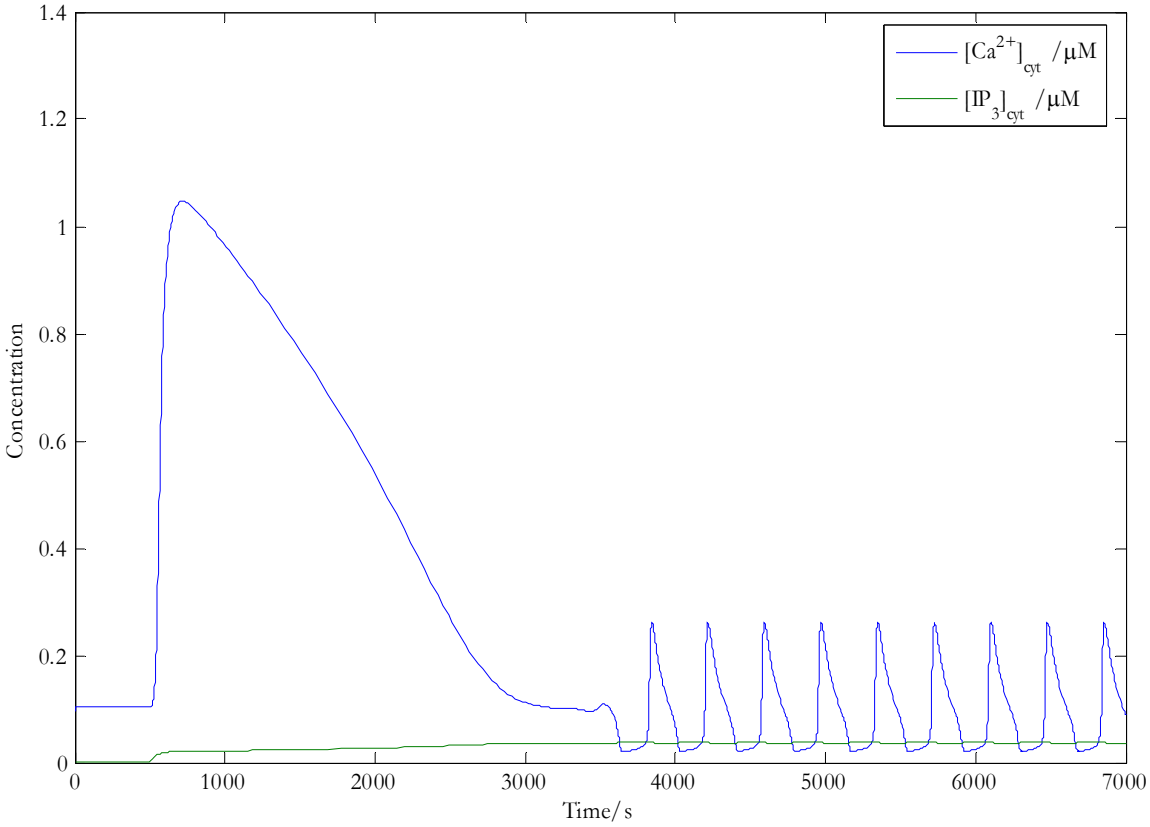

Figure A.2 The figure created by the script is presented here.

A.4 References

1. Hucka, M., et al., *The systems biology markup language (SBML): a medium for representation and exchange of biochemical network models.* Bioinformatics, 2003. **19**(4): p. 524-531.
2. Finney, A. and M. Hucka. *Systems Biology Markup Language (SBML) Level 2: Structures and facilities for Model Definitions.* 2003 [cited 2005 June 8]; Available from: http://www.sbml.org.
3. Keating, S.M. *SBML Toolbox User's manual.* [cited 2005 June 8]; Available from: http://www.sbml.org.
4. *The Matlab documentation.* 2003 [cited 2005 May]; Available from: http://www.mathworks.com/access/helpdesk/help/techdoc/matlab.html.
5. Schaff, J., et al. *The Virtual Cell Portal.* [cited 2005 May]; Available from: http://www.vcell.org.